

Avalanches, climate and glaciers -  
a reconstruction based on lake sediments from  
lake Kjøsnesfjorden

by Stephan Amm

Master thesis in Earth Science



Department of Earth Science

University of Bergen

March 2023



## Abstract:

Two lake sediment cores from Kjøsnestjønden, Western Norway, have been analysed to examine the glacier history and mass wasting processes during the Holocene. Previous research, climate data and a quaternary geological map were used to gain further understanding.

A detailed sedimentological analysis was done, including measuring magnetic susceptibility, loss-on-ignition, XRF core-scanning, X-Ray CT scanning, and Principal Component Analysis. A bathymetrical survey and CHIRP profiling were performed to acquire geomorphology information. An age-depth model using calibrated radiocarbon dates was established.

Based on multi-proxy analysis, the lithostratigraphy and the age-depth model, three slope processes (snow avalanche, glaciofluvial and fluvial) could be identified for the sedimentological record of core 603-21-01 PC. The results show nine snow avalanche events were discovered, by increased number of coarse-sized particles in the lake sediment core, and seven of them occurred during the Little Ice Age.

This project's second aim was to study the glacier history of Jostedalbreen and Grovabreen. After the sediment and XRF-analysis, a Principal Component Analysis was performed to distinguish between minerogenic and non-minerogenic units in core 603-21-08 PC. The results showed the element Titanium being a good proxy for glacier activity. The examination showed increased glacier activity from 7800 to 7900 years, during the "Finse-Event". A decline directly after was followed by a steady increase in activity from 7000 yrs. BP until the 1990s, when the glaciers started retreating again. The findings from this project show a glacier history record similar as earlier reconstructions. It differs by suggesting an earlier glacier readvance at 7000 yrs. BP and suggesting the presence of at least a small glacier on the Jostedalbreen plateau.

# Forord

To kjerneprøver fra Kjøsnesfjorden, Vestland, har blitt analysert for å undersøke den glasiale historien og massebevegelser i holocen. Tidligere undersøkelser, klimatiske data og et kvartærgeologisk kart ble brukt for å få en dypere forståelse av prosessene i området.

En detaljert sedimentologisk analyse, inkludert målinger av magnetisk mottagelighet, glødetap, XRF-kjerneskaning, røntgen CT skanning, og hovedkomponentanalyse (PCA) har blitt gjennomført. En batymetrisk undersøkning og CHIRP profiler ble studert for å undersøke geomorfologien i Kjøsnesfjorden.

Basert på multi-proksianalyse, litostratigrafien og alder-dybde modellen har tre avsettende agenser blitt identifisert (snøskred, glasifluviale- og fluviale prosesser) i kjerneprøve 603-21-01PC. Resultatet viser at ni snøskredhendelser, syv under «lille istis» ble oppdaget av et økt antall grove partikler i kjerneprøven.

Dette prosjektet sitt andre mål var å undersøke den glasiale historien til Jostedalsbreen og Grovabreen. Etter sediment og XRF-analysen, ble hovedkomponentanalyse (PCA) utført for å skille mellom minerogene og ikke-minerogene enheter i kjerne 603-21-08PC. Resultatet viste at Titan var en god proksi for glasial aktivitet. Undersøkelsen viste en økt glasial aktivitet fra 7800 til 7900 år før nåtid, under «Finse hendelsen». En brå nedgang i aktivitet etter «Finse hendelsen» ble etterfulgt av en gradvis økt aktivitet fra 7000 år før nåtid fram til på 1990-tallet, da breene starta å trekke seg tilbake. Det glasiale signalet fra kjerneprøvene undersøkt i dette prosjektet viser lignende utvikling som fra andre studier i området. Forskjellen er at det blir foreslått et tidligere breframrykk ved 7000 år før nåtid, og at det var en liten isbre på Jostedalsbreplatået.



## Acknowledgements:

First, I would like to thank my supervisors Jostein Bakke, Torgeir Opeland Røthe and Eivind Nagel Støren for giving constructive comments, technical assistance guidance and support during my master project.

Also, a special thanks to Jan-Magne Cedarstrøm, Benjamin Robson and Kristian Vasskog, who were there during the field survey and help me in the Earthlab, assisted with ArcGIS and answered my questions, whenever they occurred.

A special thanks goes to Emilie Randeberg and the Department of Earth Science for providing a great academic environment.

I would also like to thank the lunch group, many of which also helped in the GEOV226 field and lab course, at the mammoth, Anna de Bode, Isaac Dawson, Hilde Mangerud, Mara Sternberg, Marcos Tirado and Holly Tolson for good talks, parties and trips.

A special thanks goes to lunch table regulars and friends Severin Skattum and Sverre Soldal for their help in the lab, with ArcGIS problems and improving this thesis. The regular trips and parties are highly appreciated.

I would like to thank my family and friends for their ever-lasting support during the last years.

Finally, I would like to thank my daughter Wilhelmine for giving me smiles and hugs, when I needed them and my wife Antonia Thurmaier for being there for me and supporting me in every possible way. Thank you.



## Contents

1. Introduction .....	3
1.1. The significance of lake sediments to reconstruct the climate.....	3
1.2. Objective .....	6
2. Background Information .....	8
2.1. General description of Kjøsnesfjorden.....	8
2.2. Geological Background .....	10
2.2.1. Bedrock Geology .....	10
2.2.2. Quaternary Geology along Kjøsnesfjorden .....	11
2.3. Drainage History of Kjøsnesfjorden .....	12
2.4. Climate in the study area .....	14
2.4.1. Regional climate.....	14
2.4.2. Previous work in the area and the climate history in the Holocene .....	18
2.5. Slope processes and lake sediments.....	22
2.6. Landslide and avalanche history in Kjøsnesfjorden .....	25
3. Methods.....	27
3.1. Field Methods .....	27
3.1.1. Bathymetry .....	27
3.1.2. Seismic survey.....	28
3.1.3. Coring.....	28
3.2. Laboratory Methods .....	29
3.2.1. Logging .....	30
3.2.2. XRF – scanning .....	30
3.2.3. Magnetic Susceptibility (MS).....	32
3.2.4. Loss on Ignition (LOI).....	32



3.2.5.	CT-scanning .....	33
3.3.	Dating Methods .....	33
3.3.1.	Radiocarbon-Dating ( <sup>14</sup> C) .....	33
3.3.2.	Age-depth-model .....	35
3.4.	Data Analysis .....	35
3.4.1.	Principal Component Analysis – PCA .....	35
4.	Results .....	37
4.1.	Results of the field methods .....	37
4.1.1.	Bathymetric map and seismic survey .....	37
4.2.	Age model .....	41
4.2.1.	Radiocarbon dating results .....	41
4.2.2.	Core 603-21 01 PC .....	41
4.2.3.	Core 603-21 08 PC .....	41
4.3.	Age-depth model .....	42
4.3.1.	Core 603-21 01 PC .....	42
4.3.2.	Core 603-21-08 PC .....	44
4.4.	Results of the sediment analysis .....	44
4.4.1.	Description of core 603-21 01 PC .....	44
4.4.2.	Description of core 603-21 08 PC .....	57
4.5.	Data Analysis .....	60
4.5.1.	Principal Component Analysis – PCA .....	60
4.5.1.1.	Core 603-21-08 PC .....	60
5.	Discussion .....	61
5.1.	Uncertainties .....	61
5.2.	Core 603-21-01 PC .....	62
5.2.1.	Age-depth model .....	62

5.2.2.	The interpretation of different sediment signatures .....	63
5.2.3.	Linking processes to event intervals: .....	67
5.2.4.	Summary and answer to research question: .....	70
5.3.	Core 603-21-08 PC .....	71
5.3.1.	Age-Depth model .....	71
5.3.2.	The use of lake sediments to analyse glacial activity. ....	71
5.3.3.	Interpretation of the sediment record.....	72
5.3.4.	Comparison of interpretation with previous glacier activity record .....	75
5.3.5.	Summary and answer to research question .....	77
6.	Conclusion.....	78
7.	Future.....	80
8.	References: .....	81



# 1. Introduction

Minor and major climate fluctuations have characterized the Holocene era, impacting the topography and glaciers of Western Norway (Karlén et al., 1988; Nesje & Dahl, 1991; Nesje & Kvamme, 1991; Bjune et al., 2008; Nesje et al., 2000; Nesje et al., 2001; Nesje et al., 2005; Nesje et al., 2007; Aa & Bondevik, 2022; Hesjedal, 2022). The consequences of ongoing climate change include the worldwide retreat and disappearance of glaciers (Zemp et al., 2015) and increased precipitation, leading to a rise in mass wasting events in Norway (Hanssen-Bauer et al., 2015).

Kjøsnestfjorden is a prime example of a lake affected by climate changes, as it has steep slopes, making it prone to mass wasting events, and receives glaciolacustrine sediments from surrounding glaciers such as Grovabreen and Jostedalbreen. Quaternary geology, shoreline changes, and the drainage history of Kjøsnestfjorden due to glacioisostatic rebound have been described by Klakegg (1981) and Klakegg & Rye (1990), while Hesjedal (2022) focused on avalanche deposits along Kjøsnestfjorden.

Nonetheless, there is a knowledge gap between mass wasting events and the glacial history in the study area. Therefore, the acquisition of a continuous record of paleo data – lake sediments – is crucial to understand natural climate variability in this region.

## 1.1. The significance of lake sediments to reconstruct the climate

The knowledge of the past is the key to a better understanding of our future. We live in an ever-changing environment on our planet. The Earth's climate has been changing ever since and will continue to do so in the future. Therefore, this thesis focuses on both paleoclimate as well as its consequences in shaping our current and future environment. The Holocene, ranging from 11.700 years to the present, is, geologically speaking, just a glimpse on the one hand, and on the other hand, has much to offer for Quaternary geologists and palaeoclimatologists. It is important to analyse past processes and climatic variations to understand climate change. (van der Bilt et al., 2016)



Figure 1: Kjøsnæs fjorden with steep slopes and the glacier Lundabreen in the background. Source: Stephan Amm

Both geology and climate influence the processes shaping the Earth's surface. The climatic factors are precipitation, evaporation, temperature, and wind. The geological factors are bedrock, erosion, geomorphology, and lake morphology. The typical processes are snow avalanches, glacier movement & abrasion of the bedrock, and slope processes, such as landslides, rockfall, mudslides, fluvial processes, and underwater slope processes. (Bradley, 2014)

The sediments found on lake bottoms are either autochthonous, produced within the lake or allochthonous, originating outside the lake and transported there by one or more of the already mentioned processes. The sediment composition (e.g., mineralogy or grain size) determines the on and the deposition processes. (T. Cronin, 2009).

Lakes accumulate sediment from their surrounding environment, and they can be used as an important source of information because lake sediments provide a continuous record of information that is preserved over thousands of years. After their acquisition, they are used to perform laboratory analyses to acquire high-resolution data to explore geological processes influencing the lake's depositional environment and the area's paleoclimatology (Bradley, 2014; van der Bilt et al., 2016).

One of the first scientists to use lake sediments as a source for palaeoclimatological studies was Wibjörn Karlén in 1976, who measured the organic content in glacially sourced sediment and used it as an inverse indicator of glacial activity. Lake sediments continued to be of particular interest for glaciology (van der Bilt et al. (2015), Xu et al. (2015)) and palaeoclimatology as Nesje & Dahl (2001), Nesje et al. (2000, 2001, 2005, 2007), Bakke et al. (2005a, 2005b, 2009, 2010, 2013), Bjune et al. (2005), Gjerde et al. (2018) and Røthe et al. (2019b). Previous flood events were examined in lake sediments by Støren et al. (2010, 2016) and Vasskog et al. (2011) as well as mass wasting events (such as snow avalanches) (Vasskog et al. (2011), Sletten et al., 2003, Nielsen et al., 2016, Nesje et al., 2007, Røthe et al., 2019).

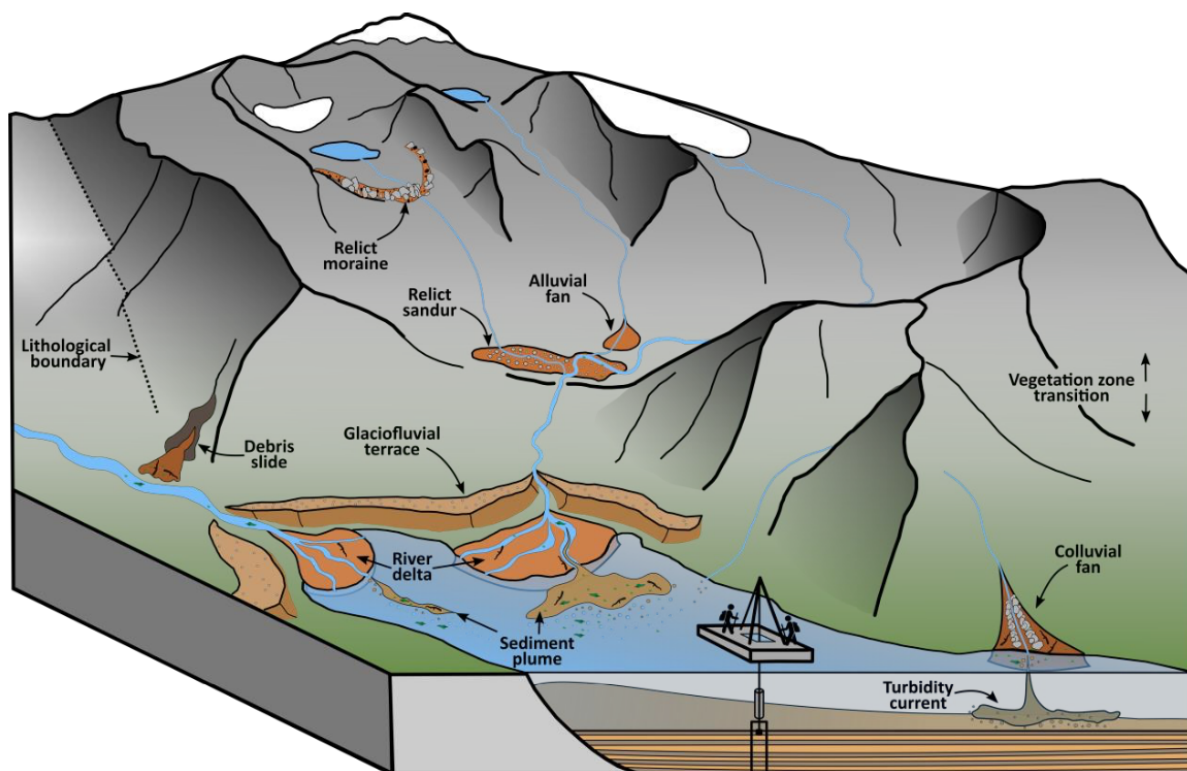


Figure 2 Shows glaciofluvial, contributing sediments to a lake's bottom. Understanding the processes on land is crucial to understand and interpret the sediment signal. Figure: Johannes Hardeng

One of those landscapes is the Jølster region in Western Norway with Jølstravatnet and Kjøsnesfjorden. It was shaped by the retreating Scandinavian ice sheet leaving steep mountain slopes and a narrow, deep lake with glaciers surrounding it behind.

The steep slopes on land and the continuation underwater make Kjøsnesfjorden prone to mass wasting processes, whose sediments can be found on the lake floor (see Figure 2).

## 1.2.Objective

This study aims to answer the overall research question: What can *lake sediments in Kjøsnesfjorden tell us about a changing Holocene climate?*

The work includes investigating and identifying the origin of lake sediments in Kjøsnesfjorden, the reconstruction of the glacial history of Grovabreen and Jostedalsbreen and the aim to link the slope processes to changes in the Holocene climate.

This study presents a multi-proxy record from Kjøsnestjønden to determine the depositional processes for the lake sediments and the glacial history. They are analysed using different techniques: x-ray fluorescence scanning, measuring the magnetic susceptibility, CT-scanner, loss-on-ignition, radiocarbon dating as well, as data analysis.

- *How has the climatic change in the Holocene caused landslides/avalanches around Kjøsnestjønden?*
- *What is the impact of the surrounding glaciers on the landslides around Kjøsnestjønden?*
- *Which sediment sources can be determined in the sediment cores?*
- *How can the bulk sediment properties of the core be used to distinguish different sediment sources and slope processes?*
- *What do lake sediments from Kjøsnestjønden tell us about the climate in the Holocene?*



## 2. Background Information

### 2.1. General description of Kjøsnesfjorden

Kjøsnesfjorden is a part of lake Jølstravatnet, located in Western Norway in the Jølster municipality, lies at 207 masl (Klakegg, 1981) and the deepest part is 140 m deep (see the bathymetric map in chapter 4).

Steep slopes surround Kjøsnesfjorden with various glaciers on the mountain plateau, most importantly, Lundabreen, right behind the village of Lunde, to the east of Kjøsnesfjorden, a part of Norway's biggest glacier, Jostedalsbreen (see Figure 3) and Grovabreen, a plateau glacier to the South of Kjøsnesfjorden with an area of 16,6 km<sup>2</sup> (Kjøllmoen et al., 2022), which also adds glacial meltwater and sediments to the fjord. (see figure 3)

The proximity to Jostedalsbreen, Lundabreen (as a part of Jostedalsbreen) and Grovabreen makes Jølstravatnet and therefore Kjøsnesfjorden a glacial lake.

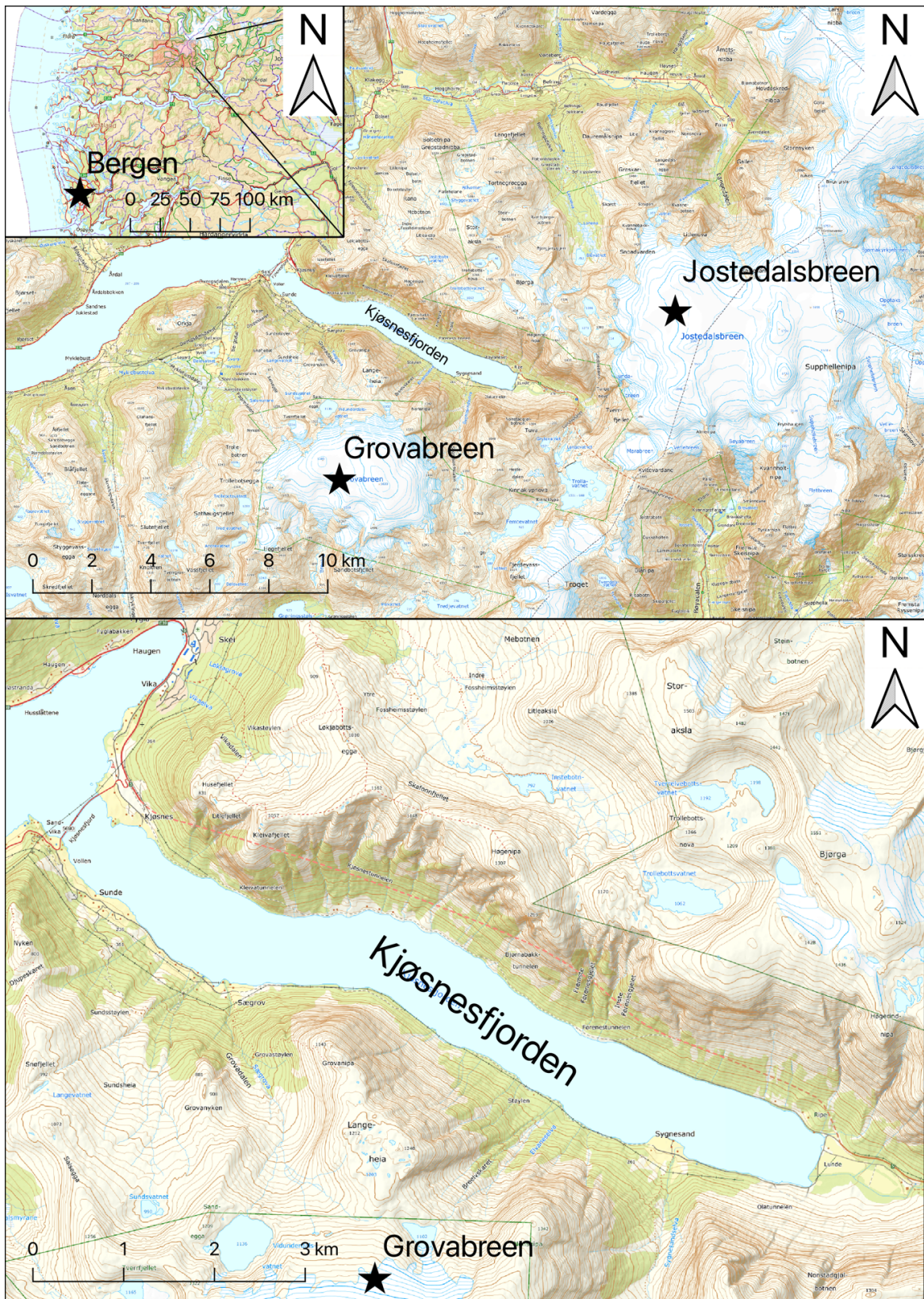


Figure 3: Location of Kjøsnestjorden: around 120 km north-east of Bergen, west of Jostedalbreen, north of Grovabreen (source: kartverket.no)

## 2.2. Geological Background

### 2.2.1. Bedrock Geology

According to the bedrock map of the NGU (Norges Geologiske Undersøkelse, Figure 4), the bedrock consists of coarse-grained quartz-monzonite, a plutonic rock (Wanvik, J.E., 1992) with equal amounts of alkali-feldspars and plagioclase with 5-20 % felsic minerals. It is often converted to eye gneiss on the south-eastern three-quarters of Kjøsnesfjorden. The bedrock of the other quarter consists of granitic orthogneiss with magmatic bands of dioritic to granitic composition and eyegneiss (see Figure 4).

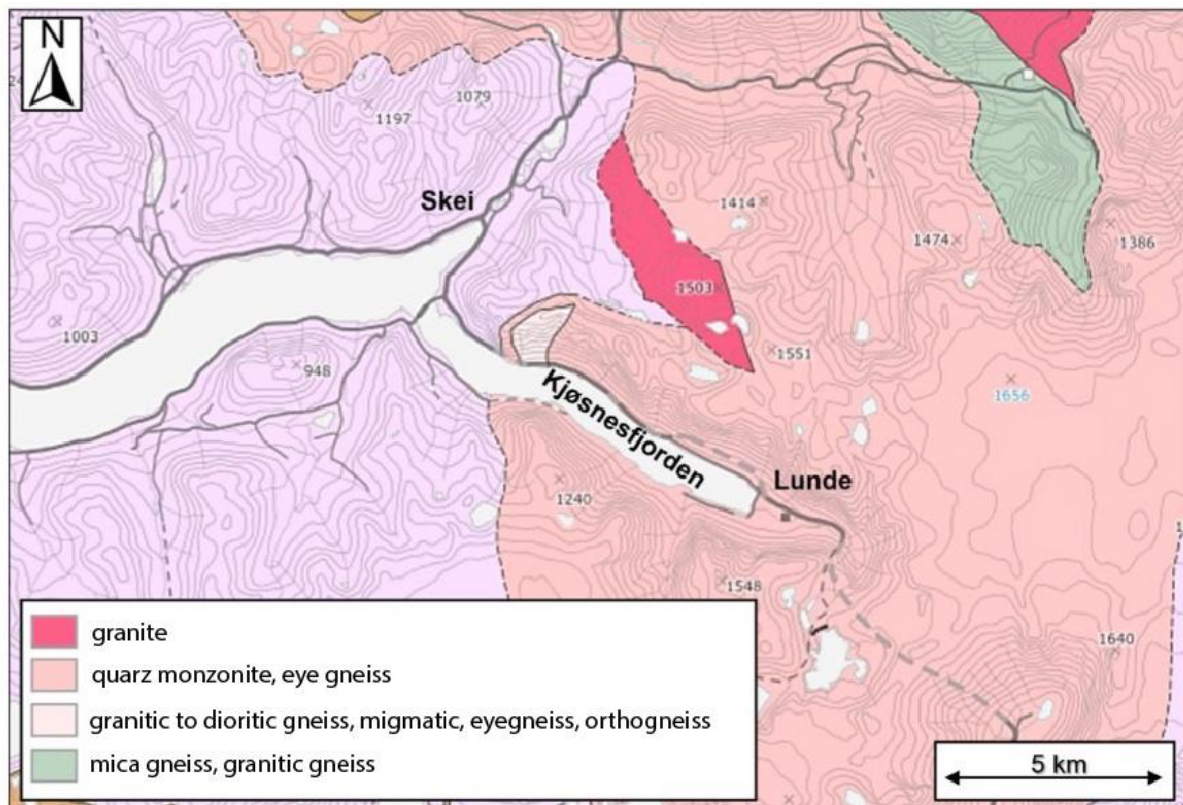


Figure 4: bedrock map of the project area; modified after Hesjedal (2022) and NGU's national bedrock database (NGU, 2022)

### 2.2.2. Quaternary Geology along Kjøsnesfjorden

The Quaternary Geology surrounding Kjøsnesfjorden is dominated by various glacial processes, such as weathering, erosion, transportation, and deposition, during the ice ages throughout the Holocene.

The Quaternary geological map (Figure 5) visualises the sediments along Kjøsnesfjorden. The present-day shoreline consists of landslide material, which has been deposited at the bottom of the slope along the fjord. Most of the slope surface is plain bedrock; therefore, the landslide's components are mainly bedrock fragments. The landslide deposits are interrupted by river deposits at Lunde in the east, where sediments from Jostedalsbreen are transported into the lake, and on the southern side of the fjord, next to Sægrov (see Figure 5), where both glacial (from Grovabreen) and river sediments are deposited. On the plateau above Kjøsnesfjorden, moraine material of various thicknesses, peat and weathered material are mapped.

Aa (1995) mapped and described the LIA moraines of Grovabreen and made a map, which has later been adapted by Seierstad et al. (2001). The original map shows the early Holocene, Erdalen event (Seierstad et al. (2001); Aa & Sønstegaard, 2018), LIA moraines, fluvial and glaciofluvial deposits, and a river fan flowing into Kjøsnesfjorden.

Given the sediments deposited along the fjord, it can be concluded that the sediments on the lake floor will be similar.

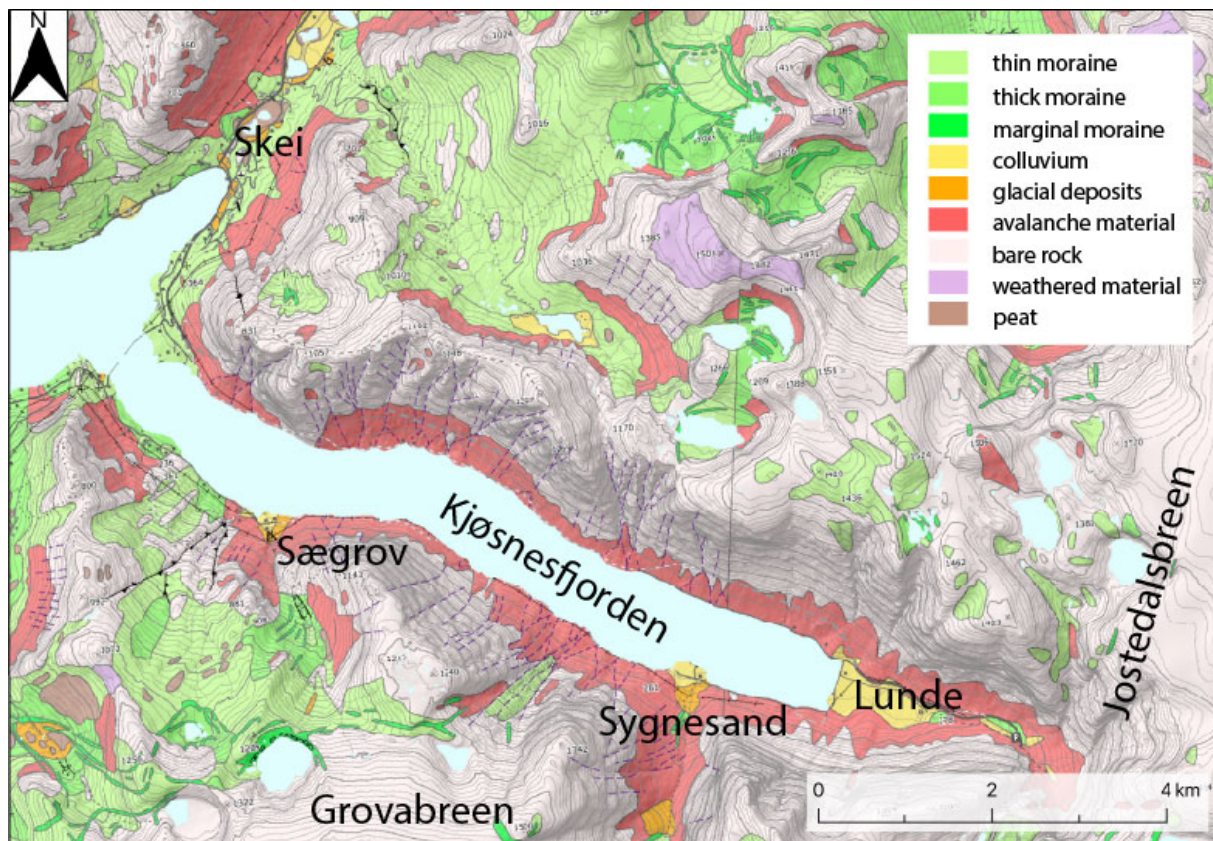


Figure 5 Shows a Quaternary geological map of the study area with avalanche and glacial deposits, and colluvium and moraine material deposited along lake Kjøsnesfjorden shore. Bare Precambrian rock is visible further up the steep slope. Modified after NGU (2023)

### 2.3. Drainage History of Kjøsnesfjorden

The geological history of Kjøsnesfjorden is closely linked to Jølstravatnet's. The lake was deglaciated during the Preboreal Chronozone, at 9500 years before the present (yrs. BP) (Klakegg, 1981).

Klakegg & Rye (1990) did a survey, combining deglaciation history, former lake levels and the stratigraphy, with lake sediments, in lake Fuglevatnet close to Skei and they discuss the tilted lake shorelines of Jølstravatnet from 9500 yrs. BP until the present situation. They divided the development into five phases; see Figure 6 for a more detailed description.

The first phase before 9500 yrs. BP, the eastern part of Jølstravatnet, which is majorly Kjøsnesfjorden, was occupied by glaciers. The retreat of the ice lobes caused an outburst of the ice-dammed glacial lake and led to the formation of the drainage outlet at Skei.

During the second phase (from 9500 to 9200 yrs. BP), ice lobes were retreating in Kjøsnestfjorden, so Jølstravatnet was a frontal glacial lake. This phase is rather essential to the development of the present state of Kjøsnestfjorden. It describes its status from being an ice-dammed lake to getting deglaciated, which simultaneously leads to glacioisostatic uplift and regression at the east of Kjøsnestfjorden (Klakegg & Rye, 1990).

Phases III, IV and V describe the post-glacial history of Jølstravatnet based on the change of the outlet at Skei via a watershed phase (IV) to the present-day outlet at Vassenden.

Lake phase III (9200 to 7500 yrs. BP) is characterized by the ice retreat, the continuation of the glacioisostatic rebound, and regression in Kjøsnestfjorden.

During phase IV (7500 to 6000 yrs. BP) the drainage happened via both outlets, Skei and Vassenden. Later during phase IV, the drainage outlet shifted totally to Vassenden and a regression of Jølstravatnet started. The end of phase IV is defined as when the highest floods are no longer traceable in lake Fuglevatnet.

Lake phase V (6000 yrs. BP to present) represents the phase, during which the outlet stays at Vassenden, the regression and the tilting of the whole lake continued. It is assumed that the tilting decelerates up to the present day.

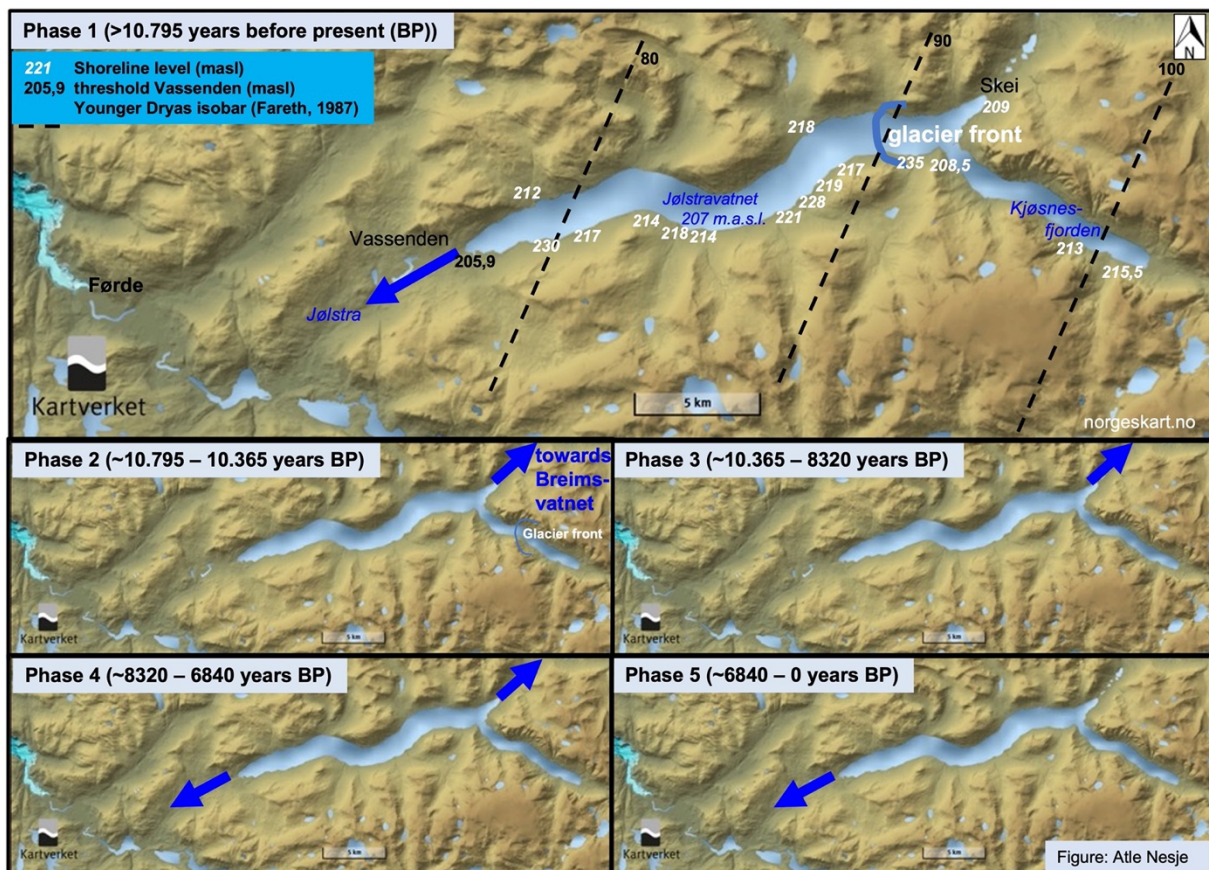


Figure 6 Drainage history of Jølstravatnet, which shows that during phase 2, the glacier was still present, and during phase 3, Kjøsnestfjorden was deglaciated. Figure made by Atle Nesje, based on Klakegg & Rye (1990).

## 2.4. Climate in the study area

### 2.4.1. Regional climate

The westerlies and the North Atlantic current influence today's climate in Western Norway transporting humid air to Western Norway, whose entrapment in the steep mountains in combination with the Gulf Stream results in heavy precipitation along the coast.

The North Atlantic oscillation (NAO) index quantifies the pressure difference between the Iceland Low and the Azores High. A positive NAO represents already an stated pattern, while a negative NAO results from the opposite pressure pattern (Hurrell, 1995; Hurrell et al., 2003). The annual precipitation measured at Skei (205 masl.) 4 km northwest of the study area, from 1970 until today is shown in Figure 7. The trendline shows a steady increase in precipitation from 1760 to 1950 mm.

Figure 8 shows the annual average temperature measured at Fjærland-Skarestad from 1970 to 2004 and at Fjærland-Bremuseet from 2006 to 2022. Those stations are located about 25 km southeast of the study area. The trendline steadily increases the average annual temperature from 5,0 to 5,9°C.

As visible in Figure 9 is the prevailing wind direction from the northwest transporting wet air from the North Sea.

Given the ocean-influenced precipitation-loaded wind from the northwest, it can be concluded that the weather is in a maritime climate zone.

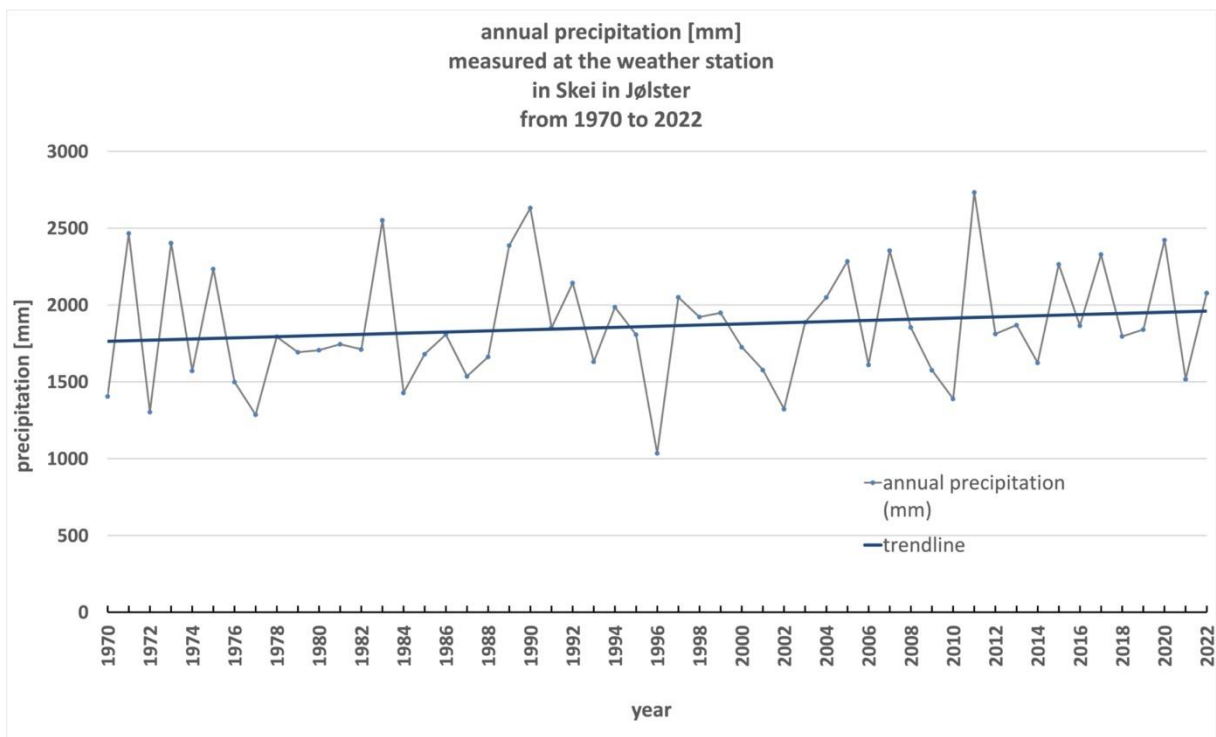


Figure 7 shows the annual precipitation from 1970 to 2022. The average (shown in the trendline) increases steadily from 1760 to 1950 mm/year. Data source: seklima.met.no (2023).



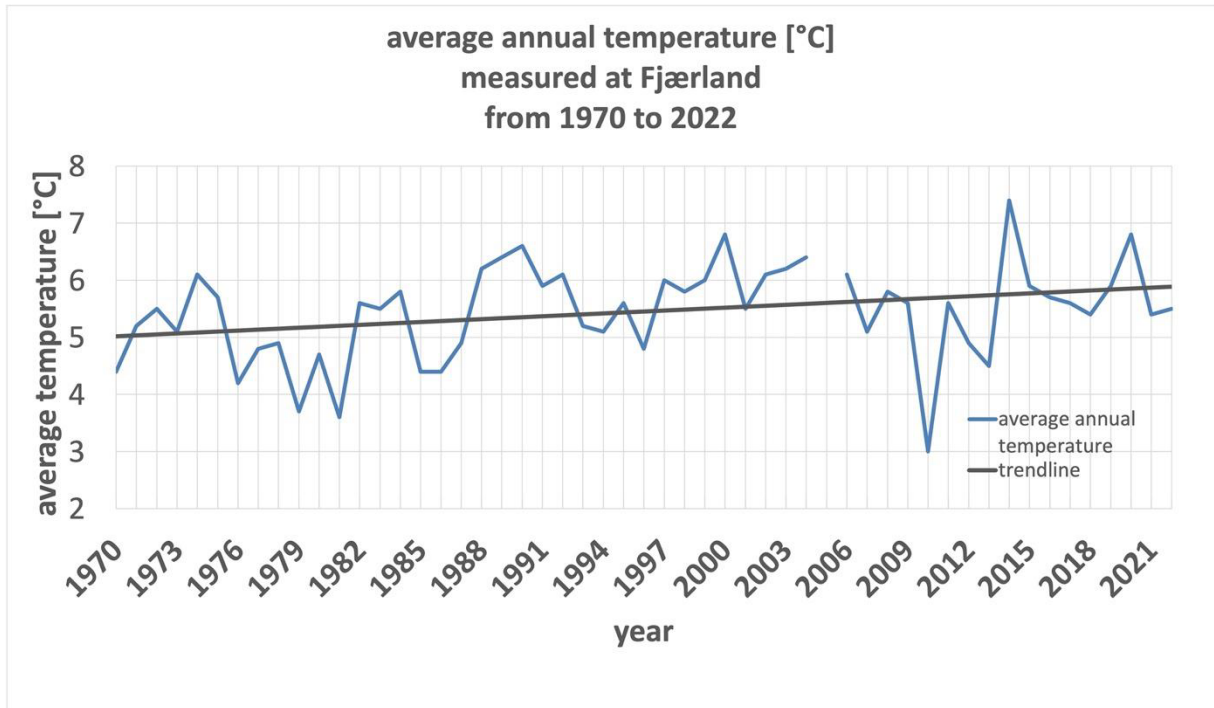


Figure 8 shows the annual average temperature measured at Fjærland-Skarestad (1970 - 2004) and Fjærland-Bremuseet (2006 - 2022). Data source: seklima.met.no (2023)

## Wind rose for RV5 Lundebotn (SN57380) from January 2016 to December 2022

Calm (0.0–0.2 m/s) = 2.5 %

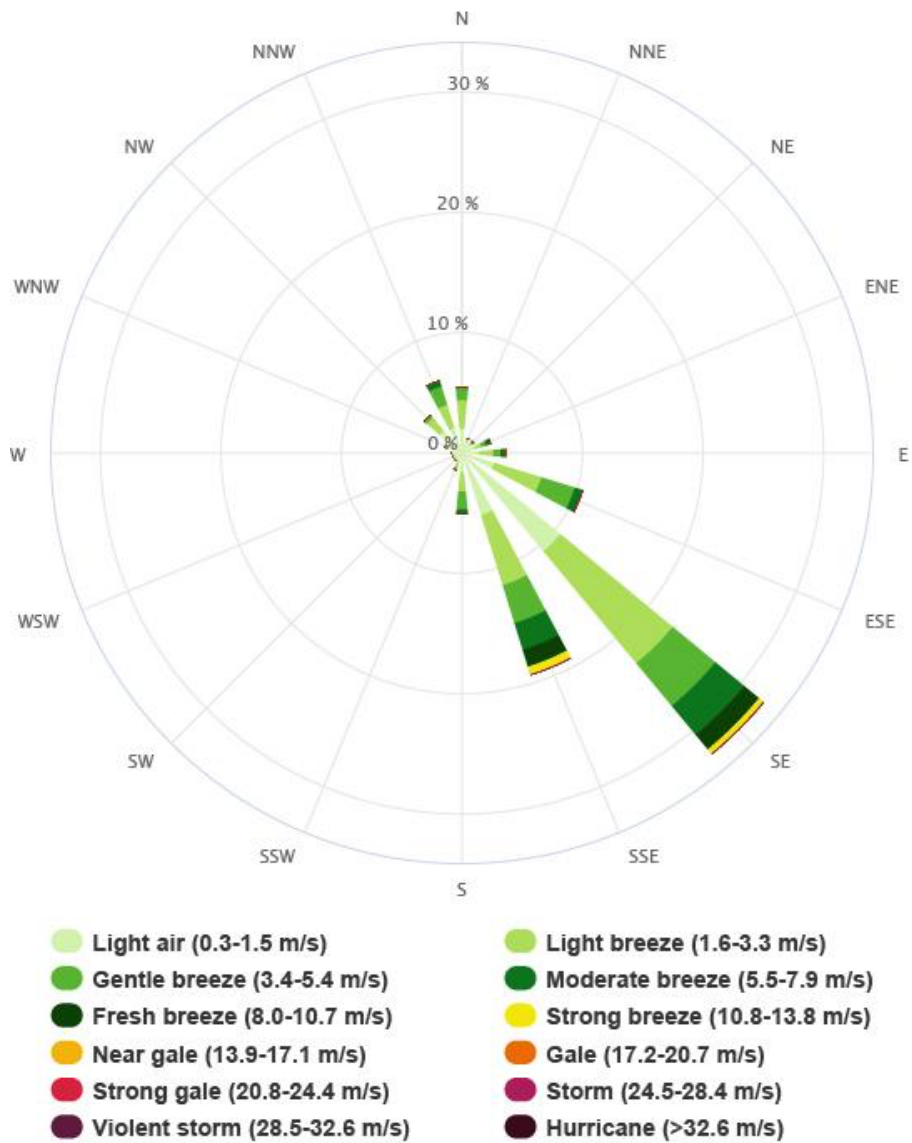


Figure 9 rose from the weather station at Lundebotn, which shows the average wind speed and direction from January 2016 to December 2022. Data source: seklima.met.no (2023)

## 2.4.2. Previous work in the area and the climate history in the Holocene

### Younger Dryas:

The Younger Dryas (12 900 to 11 700 yrs. BP (Bradley, 2014)), named after *dryas octopetala*, the most common flower during that period, was the last stage of the Pleistocene epoch.

According to Nesje (1992), cirque glaciers existed in the area during the Younger Dryas chronozone, and there were fjord glaciers depositing glaciofluvial sediments during the cold spell (Rye et al., 1987).

### Holocene:

The Holocene can be divided into early (11,7 to 8,3 ka BP), middle (8,3 to 4,3 ka BP) and late (4,3 ka to present) (Walker et al., 2019). The climate in Western Norway is characterised by large fluctuations in that period and can be reconstructed based on glacier studies (Nesje & Kvamme, 1991; Nesje et al., 1991; 2008; Nesje, 2009), and since summer temperatures and winter precipitation influence a glacier's mass balance, glaciers function as a good proxy to study the climate.

In addition to that, pollen distribution, a biological proxy, (Bjune et al., 2005), as well as the already mentioned lake sediments (Nesje et al., 2001; Dahl et al., 2002; Vasskog et al., 2011), can be used for climate studies.

Jostedalbreen (see Figure 3), mainland Europe's largest glacier, is in Western Norway in relation to latitudinal perturbations of the North Atlantic cyclone track and the atmospheric polar front (Nesje, 1992). Climatic changes during the Holocene and glacier variations can be observed there (Nesje, 1992).

### Early Holocene

#### Preboreal:

According to Bjune et al. (2005), a more oceanic climate with low July temperatures and high annual precipitation was prevailing during the early Holocene until around 8500 yrs. BP.

Bjune et al. (2005) performed pollen analysis and found out that the July temperatures rose from 8,5 °C to 10,5 °C between 11 000 and 10 000 cal. yr. BP. Berger (1978) has previously confirmed a higher than present solar radiation on land and warmer ocean water in the Northern Hemisphere.

The Erdalen event is the first evidence of glacial activity in southern Norway since the Younger Dryas. Dahl et al. (2002) observed a readvance of Nigardsbreen (an Eastern outlet glacier of the Jostedalbreen plateau), suggesting that the Erdalen event happened in two phases: the first 10 100 to 10 050 cal. yrs. BP and the second phase are close to 9700 cal. yrs. BP, which concurs with Rye et al. (1987).

The deglaciation started during the mid-Preboreal (9500 +/- 200 y BP), occurred in the form of vertical wastage, which indicates that the ELA (Equilibrium line altitude) was above the summit plateaus (Rye et al., 1987) and continued in the valleys surrounding Jostedalbreen during the latter half of the Preboreal Chronozone (Rye et al., 1987, Nesje et al., 1991, Nesje, 1992). The temperatures were about four degrees higher than today.

#### Middle Holocene:

##### Finse-Event:

The "Finse event" at 8200 yrs. BP is a cooling event which resulted from a large meltwater impulse when the Laurentian ice shield collapsed (Barber et. al, 1998; Matero et al., 2017).

The thermohaline circulation is sensitive to freshwater input, which can cause climatic anomalies.

This sudden climatic fluctuation occurred between 8400 and 8000 yrs. BP, when the temperature dropped up to 8 °C (in Greenland) at marine and terrestrial sites around the North Atlantic Ocean (Barber et al., 1999).

Nesje et al. (2005) have concluded two glacial episodes, one at about 8200 cal. yrs. BP and one at 7900 cal. yrs. BP. During the period from 8200 to 7900 cal. yrs. BP, the July temperatures generally dropped. Both January temperature and precipitation were relatively high. They suggest that the increased glacier activity at 8200 cal. yrs. BP comes from increased winter storminess that caused more precipitation like a positive North Atlantic oscillation index (Nesje et al., 2005). In the second glacial period at 7900 cal. yrs. BP, the average summer temperatures cooled by approximately 1 °C.

Seierstad et al. (2001) took two cores (see Figure 9) from Grøningstølsvatnet next to Grovabreen to reconstruct the Holocene and glacial history as well as the local snow-avalanche activity. The glacier was melted away between 9470 cal. yrs., BP and 4700 cal. yrs. BP, except for a short period from 8420 to 7880 yrs. cal. BP, which can be correlated with the "Finse event".

Nesje et al. (1991) present lake sediment data from Vanndalsvatnet, a glacier-fed lake from Jostedalsbreen, and discuss the Holocene and climate history in that area. Nesje et al. (2005) take a closer look at the data again and present the core Vanndalsvatnet 01-2 focusing on the 8200 cal. yrs. BP event.

#### Holocene Thermal Maximum (HTM):

"Holocene thermal maximum" (HTM) from 8200 y to 5400 y BP (Gjerde et al., 2018),

According to Renssen et al. (2012), the "Holocene thermal maximum" is commonly associated with an orbitally forced summer insolation maximum. They also state that the timing and magnitude vary across the Northern hemisphere.

During the HTM various pollen records of pine, elm, and birch show that a temperate climate in the Jostedalsbreen region prevailed from 9000 to 6000 y BP. (Kvamme, 1989)

Nesje & Kvamme (1991) conclude that the ice cap on the Jostedal plateau was probably melted during the HTM (see Figure 10).

#### Late Holocene:

##### Neoglaciation:

Palynological studies performed by Kvamme (1989) show a decline in alder pollen at 6300 y BP caused by a climatic deterioration following the HTM. The birch pollen record shows an expansion from 5300 yrs. BP at the sacrifice of mainly alder and pine. This has been interpreted as the initial glacier formation due to colder climate (Nesje, 1992). This theory is proven by an extensively studied paleosol, buried by the outer LIA moraine at Haugabreen and shows a shift at 5200 y BP to colder and wetter climate (Caseldine and Matthews, 1987).

The tree line dropped below 660 m between 3600 and 3300 yrs. BP, it remained there until 750 yrs. BP, except about 2600 and 2200-2000 yrs. BP, where it was higher (Nesje, 1992).

Nesje et al. (1991) examined a stratigraphic section in the Stryn valley at an altitude of 730 m (the modern birch tree line), which revealed a 1,7 m of peat with tree stumps combined with sand and silt. The dating of a weakly laminated sand/silt horizon gave a result of 3710 +/- 50 yrs. BP (2210 - 2040 BC) and 3100 +/- 90 yrs. BP (1500 - 1260 BC), which is interpreted as seasonal/annual rhythmic glaciofluvial sediment transport (Nesje et al., 1991). A 600-year-

long Neoglacial period, the first in the Jostedalsbreen region, is represented by that record. The study shows that the ELA during that phase was 30-70 m above present (Nesje et al., 1991).

Nesje et al. (1991) studied lacustrine sediments, also showing turbidity currents entering the lake probably caused by short-lived climatic events and/or large seasonal meltings, at Vanndalsvatnet, which at present drains east of Jostedalen, and discovered that the glacier was not present from 8000 to 6100 y BP (Nesje, 2009).

Nesje & Dahl (1991) surveilled a 130 cm gully section in the drainage area of Bevringsdalen, at the south-western margin of the Jostedalsbreen ice cap, which showed late Holocene minerogenic sedimentary units, consisting of blueish-grey and sand/silt with a texture, which is similar to glacially eroded rock flour, showing glacial meltdown and peat, representing periods of little or no glacial activity, along a meltwater stream, draining two minor glaciers further up the valley.

Grovabreen regrew after 4700 yrs. BP and is still present today (Seiersted et. al., 2001).

The Medieval warm period was lasted from about 900 to 1200 AD (1100 to 750 cal. yrs. BP) (Bjune et al., 2008) marks a period with mild climate in the Northern Hemisphere.

#### Little Ice Age (LIA):

The cause for the last glacial expansion in the early 18th century in western Norway were mild and humid winters in combination with high snowfall on the glaciers (Nesje et al., 2001; Nesje & Dahl, 2003; Nesje et al., 2008; Nesje, 2009).

According to Aa (1995), some of the LIA moraines deposited by Grovabreen exceed and overlay those deposited in the early Holocene.

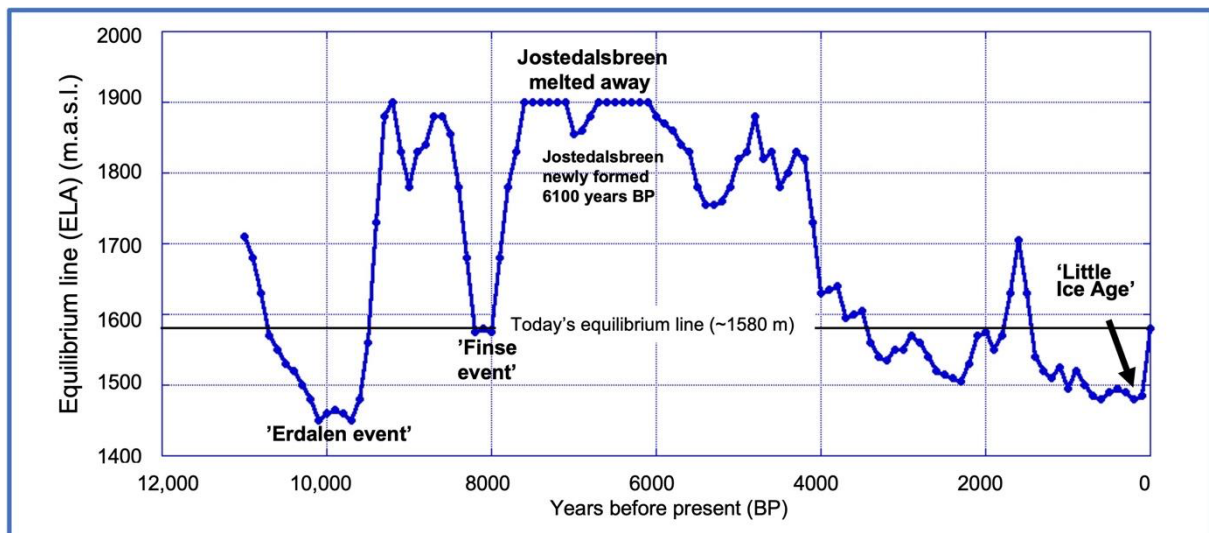


Figure 10: Jostedalsglacier ELA curve (top); figure created by Atle Nesje based on Nesje et al. (2001), Nesje (2009) and Vasskog et al. (2012).

## 2.5. Slope processes and lake sediments

### Floods:

A flood is usually triggered when there is more precipitation than on average and a river can transport. This leads to mass particle transport and strong erosion to the river's outlets, such as lakes (Sabatier et al., 2022).

Once the sediment-laden suspension arrives at the lake, the in-lake distribution depends on the density, which were described by Strum & Matter (1978) and summarized by Sabatier et al. (2022):

- Overflow: if the incoming sediment-laden water is less dense than the lake surface, it dissipates at the surface  
Sediments: continuous or background sedimentation
- Interflow: if the incoming water is denser than the surface, but less dense than the lake bottom, it follows the thermocline  
Sediments: Fuzzy base and top silty layers (see Figure 11)
- Underflow (turbidity current): if the incoming water is denser than the lake bottom water it, flows along the lake bottom.

Sediments: Either fine-grained turbidites (in large lakes or distal deposition positions) or a sediment column with a sharp (sometimes erosional) base, followed by well-sorted sand, well-sorted silt, and a clay cap.

- Homopycnal flow: if the incoming current enters a non-stratified lake and the two fluids have the same density, the sediment dissipated within the whole water column (Sabatier et al., 2022)

Sabatier et al. (2022) also state that debris flows entering a lake can evolve into turbidity currents and therefore, the resulting sediments share similarities with flood deposits (see Figure 11 below).

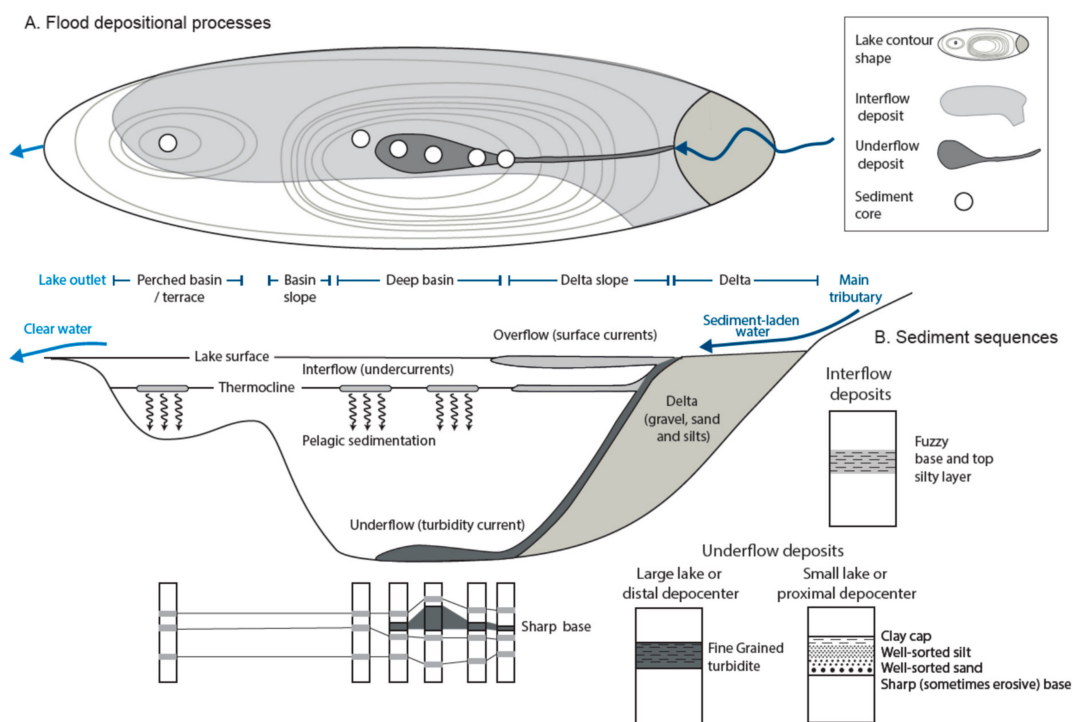


Figure 11: flood depositional process and the lake sediments from Sabatier et al. (2022)



## Glacial Lake Outburst Floods (GLOF):

Those often-catastrophic events are also known as jökulhlaups.

In general, the formation of ice-dammed lakes starts with the accumulation of water initiated by precipitation, seasonal melting and/or geothermal heating. That water body must be sealed by either bedrock, moraines and/or glacier ice. The water keeps accumulating in cavities and channels under the glacier itself. With continuous supply of fresh- and meltwater, the ice-dammed lake keeps growing.

Eventually the hydrostatic pressure exceeds the formation strength of the ice-dam and a Jökulhlaups occurs (Cuffey & Paterson, 2010).

GLOF deposits in lake sediments can be recognized by two parameters: grain size and total organic carbon (TOC). Sabatier et al. (2022) states two likely sediment sequences (see Figure 12 below). The first is a sandy turbidite, which is coarser than the background sediment, organic-poor and fining upwards. The second one is a mud layer, finer than the background sediment and organic poor.

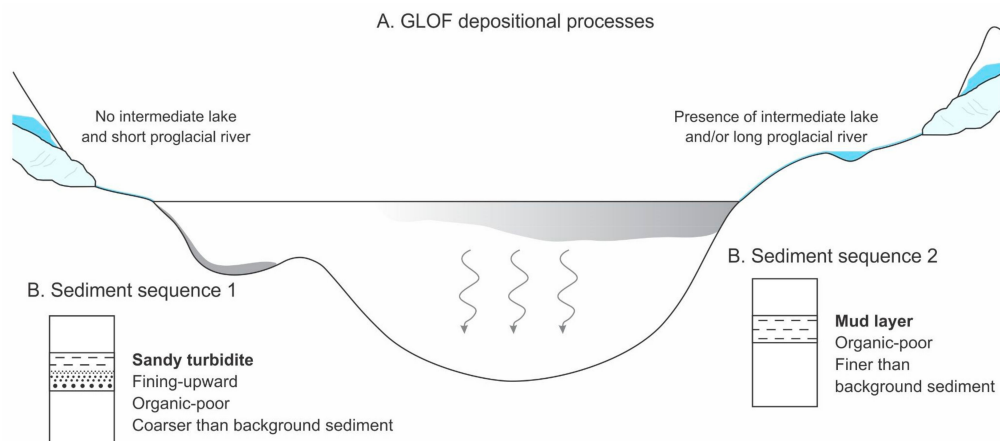


Figure 12: Glacial lake outburst flood depositional setting and sediment sequences. Source: Sabatier et al. (2022)

## Snow avalanches:

Nesje et al. (2007), Seierstad et al. (2001) and Vasskog et al. (2011) have used lake sediments to analyze the debris a snow avalanche transports to a lake. This is usually characterized by coarse to very coarse minerogenic particles and plant remains (Sabatier et al. (2022)).

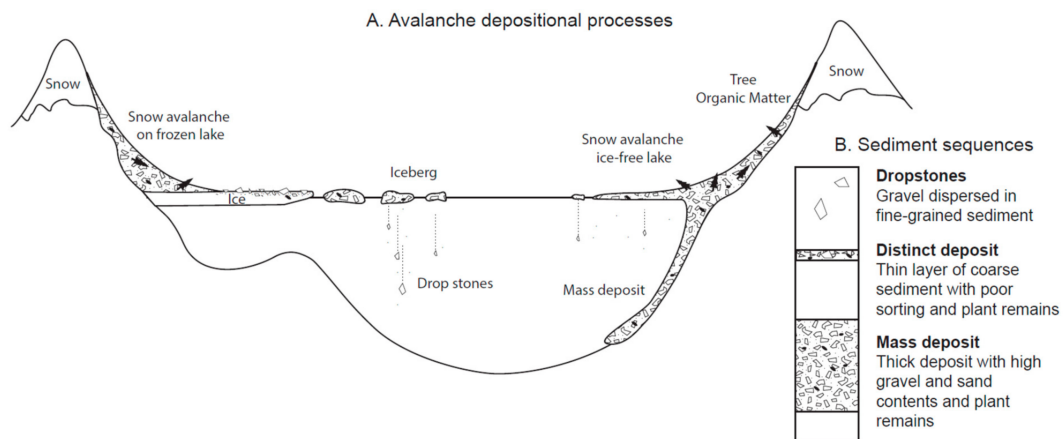


Figure 13: Avalanche depositional setting and lake sediment. Source: Sabatier et al. (2022)

## 2.6. Landslide and avalanche history in Kjøsnestfjorden

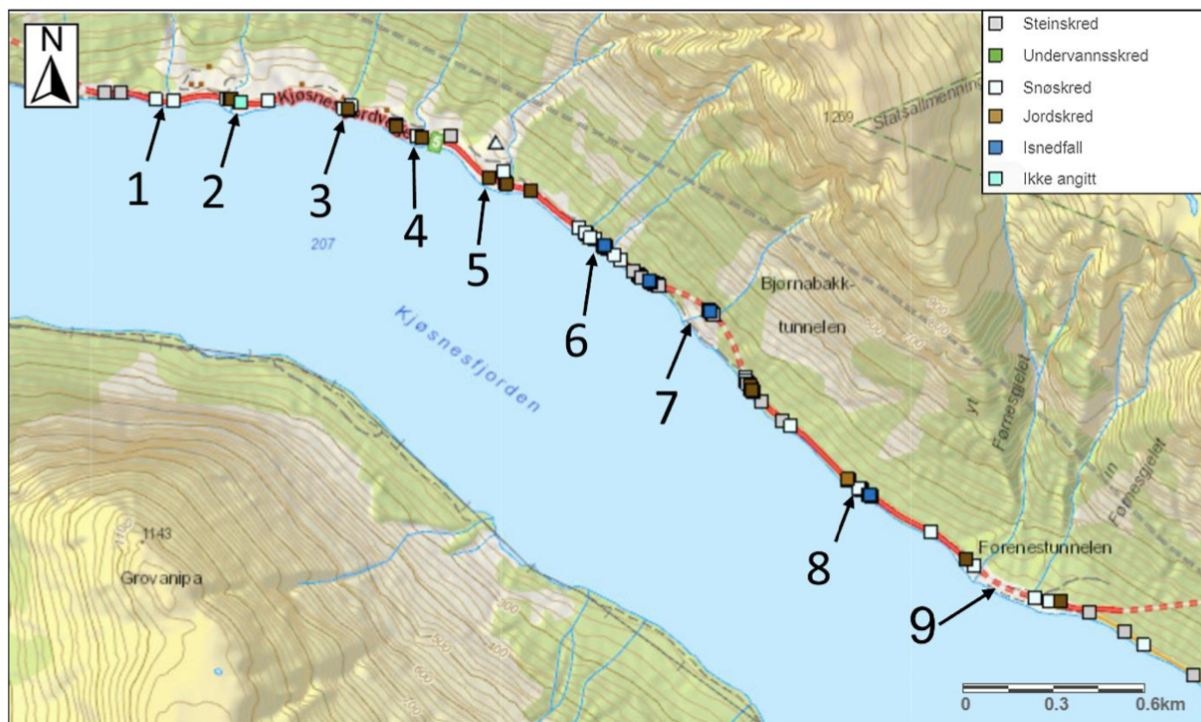


Figure 14 gives an overview about the mass wasting events, which have been recorded by the NVE in the last 35 years. Of the 118 recorded events are 56 snow avalanches, 23 were rock avalanches events, 18 were rockfall events, 15 were landslides and 2 slush avalanches

Those events led to the building of various mitigation measures, such as fences, and tunnels along Kjøsnesfjorden (Hesjedal, 2022).

According to a local farmer, we were talking to during the field trip at Lunde, the road from Fjærland to Skei got blocked by snow masses and trees, transported by snow avalanche in March 2020.

## 3. Methods

The following chapter will introduce the field methods and analytics done in the sediment laboratory. This includes methods to distinguish and date the different layers in the lake sediment cores.

### 3.1. Field Methods

In October 2021, during the GEOV226 & GEO313 field course, the relevant field work for this thesis, bathymetric mapping, CHIRP mapping and coring were performed.

#### 3.1.1. Bathymetry

Bathymetry is defined as the measurement of depths in oceans or lakes.

Before the bathymetric map created during this survey in 2021, the only available one was from 1970, created by the NVE (Norwegian water and energy directorate), and used to get an orientation for this survey.

Mapping a lake's bathymetry is crucial to understanding the processes that influence lake sediments and therefore identifying ideal coring spots. The sediment-thickness will be the thickest at the deepest point of a lake because over time, the sedimentation has gradually levelled the topography of the basin. That point is also the least affected by erosion, so the chances of getting a continuous sediment record are very high (Gilli et al., 2013).

In lakes with more complex morphology, the use of light seismic equipment such as ground penetrating radar (GPR) (electromagnetic pulses) or CHIRP (sound waves) is advantageous.

For this bathymetric survey a single echo sounder of the type "Lowrance Elite T12" was used to map the depth conditions. The surveys were performed with an inflatable boat and an outboard engine. A built-in 10 kHz internal high-sensitivity GPS-antenna, built into the echo sounder, was used to automatically locate the measurements on the chart plotter in the echo sounder. A total distance of 68 733 m bathymetric mapping was done.

The bathymetric map was created in ArcGIS Pro (provided by UiB) using an "inverse distance weighting" and the "topo to raster", with standard settings, interpolation.

### 3.1.2. Seismic survey

CHIRP (Compressed High-Intensity Radiated Pulse), as well as Bathymetry, are methods used to gain information about underwater topography, but in addition to this, CHIRP also gives us information about the stratigraphy. This survey used an Edge Tech 3100 floating below the water surface behind an inflatable boat with an outboard engine. The CHIRP works by sending out sound waves which travel at different types of frequencies (4-24 kHz) through different materials. The returned signal is then processed with a pulse compression filter to create high-resolution images of the bottom. The data was visualised using the SeiSee freeware (Version 2.22). Materials in the ground reflect the waves based on density differences. The finer the material is, the deeper the ground penetration is possible. The profile gives valuable information about the lake floor, which can be used to find optimal spots for taking sediment samples.

### 3.1.3. Coring

Table 1: Overview about the GPS position, water depth, length, and coring device of each core used for this project.

<b>Core ID</b>	<b>Longitude</b>	<b>Latitude</b>	<b>Water depth (m)</b>	<b>Length (cm)</b>	<b>Coring Device</b>
603-21-01 PC	6,494074° E	61,541234° N	112 m	270 cm	Piston corer
603-21-08 PC	6,512333° E	61,539865° N	71 m	239 cm	Piston corer

During the coring operation, a total of nine cores (four piston cores and five gravity cores) were taken from a raft during ice-free conditions. Core 603-21-01 PC and core 603-21-08 PC are used for this thesis.

The whole coring operation has been done on a raft using a piston corer for lacustrine sediments (Nesje, 1992) and a gravity core device (UWITEC). According to Nesje's description, the piston corer consists of a corer head, a stainless piston wire rope, a weight with static ropes for lifting and lowering, a piston (three pieces with a central bolt and two sealing rings), wire clamps, a core catcher and a jack. An orange-coloured PVC tube with a diameter of 11 cm and a length of 6 m was used.

To obtain the sediments, the sampler is lowered to the lake floor and hammered into the sediment until the resistance gets too high. Then, a vacuum on top of the sampler keeps the sediment. Immediately after the core is out of the water, arrows showing "up" are drawn on the PVC tube. It's crucial to store and transport the cores vertically in the correct orientation not to disturb the sediments. A saw was used to shorten the tube according to the length of the obtained sediment. After the sediments have had time to consolidate, they can get split open them for further analysis.

The UWITEC gravity corer (Uwitec USC 09000) works like the piston corer (Nesje, 1992) but is limited in terms of penetration depth, and the sampling tubes are usually shorter, made of transparent PVC and thinner (inner diameter = 86 mm) than those of the piston corer. The length of the sampling tubes is about 10 cm more per end in addition to the sample lengths (see Table 1). A green foam is used to seal the sample within the sampling tube. Unlike with the piston corer, with the gravity corer, it is possible to collect undisturbed samples of the top layers because the applied pressure by the gravity corer is lower than that of the piston corer.

### 3.2. Laboratory Methods

In this section, an overview of the laboratory techniques utilized for analysing the sediment cores is provided. Initially, the cores were divided into two sections: a reference core labelled as "REF" and a working core marked as "W." To facilitate measurements, a measuring tape was utilized, and upward-pointing arrows were drawn on each section of both cores. Subsequently, the cores were stored in a cooling room with a temperature of approximately 4 °C at UiB for future use.

The reference cores are used for XRF-scanning, MS measurements and CT-scanning. The working cores were used for LOI-sampling and macrofossil picking for C-14 dating.

Table 2 gives an overview about the laboratory methods used on each core (x = performed)

<b>Core</b>	<b>Logging</b>	<b>XRF-scanning</b>	<b>MS</b>	<b>C-14</b>	<b>LOI</b>	<b>CT-scanning</b>
<b>603-21-01 PC</b>	x	x	x	x	x	x
<b>603-21-08 PC</b>	x	x	x	x	x	x (on part 2 of 2)

### 3.2.1. Logging

Visual core logging is one of the most important yet very basic tools. The following features and elements are described cm by cm: sediment type, color (Munsell & Color, 1951), visible structures, and general description. This basic description, especially the depth scale, is very valuable for properly plotting the lab data. The plot can then be digitalized and combined with the CT scan as well as other analysis results.

### 3.2.2. XRF – scanning

An ITRAX X-Ray fluorescence core scanner was used to measure the chemical composition of the various layers in the core (see Figure 15 below). This non-destructive method creates a continuous high-resolution record (Croudace et al., 2006). For this analysis, an interval of 2 mm, a voltage of 32 kV and an amperage of 30 mA was chosen for each core. A molybdenum (Mo) tube was used as the radiation source for this analysis. The principle of this method is that an X-ray beam ionizes atoms in a sample and a detector detects the occurring fluorescence radiation. This radiation is characteristic for each chemical element.

The wet cores were covered with a thin plastic film to prevent them from drying out. The ITRAX-X-Ray fluorescence scanner takes an optical picture of each core it scans, which can be saved and used later.

The result, which is affected by sediment properties such as, water content, organic content, grain size and mineralogy, is given in cps (counts per second) and, in combination with other parameters or as ratios of two elements, can be used in geosciences. Croudace et al. (2006) states the ratio "Zr/Rb" to be used as a sediment provenance indicator on the base of turbidites, as it can give a positive signal there as well as "Mn/Ti" is a good indicator for redox-related diagenesis.

An important proxy for glacial mass turnover is the XRF signal of Ti (Bakke et al., 2009; van der Bilt et al., 2017). Wittmeier et al. (2015) observed that glacially eroded sediments feature high Ca, Fe and Ti values combined with a low 77K/293K ratio.

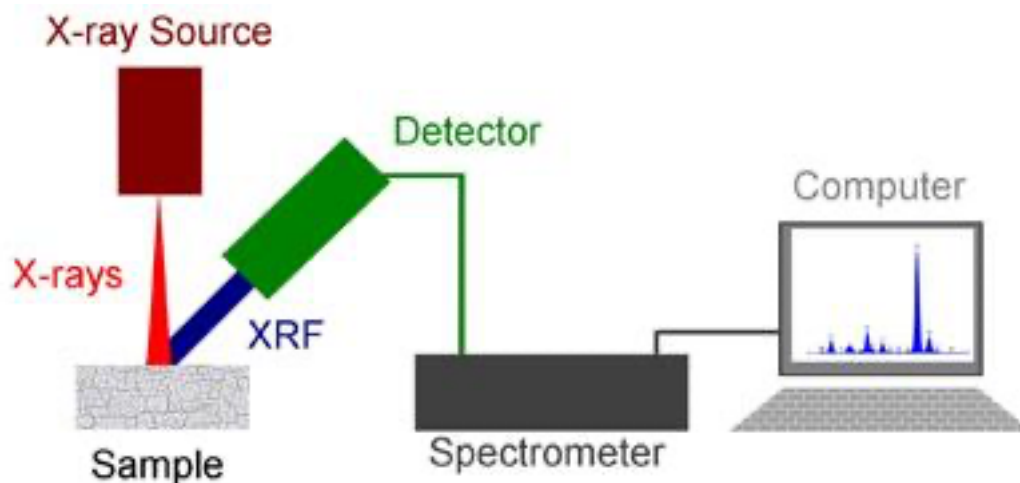


Figure 15 shows an illustration of the XRF-scanner and the path from the X-ray-source to the sample, the detector, and the spectrometer. After the analysis, the results can be viewed on a computer. (Source: <https://physicsopenlab.org/2016/02/24/diy-xrf-spectrometry/>)

The output data of the XRF-analysis are "counts per second" (cps) and is considered being semi-quantitative due to possible scattering or absorption caused by downcore changes in mineralogy, grain size, water content and surface roughness, which all influence the precision of the measurements (Croudace et al., 2006).

One method to easily improve the interpretation and decrease scattering effects is by normalizing the data. The element data is divided by incoherent plus coherent scattering to remove instrumental effects (Kylander et al., 2011).



The results of the XRF analysis have been resampled to a 4 mm spacing, the same as the MS analysis.

### 3.2.3. Magnetic Susceptibility (MS)

Magnetic susceptibility (MS) is a dimensionless parameter that can be explained by the amount of magnetization acquired by a material in response to a weak magnetic field (R. Thompson, 1975; Støren et al., 2016). A GEOTEK multi sensor core logger was used to find the contrasts in the magnetic properties in different depths of the sediment core. The magnetic susceptibility was measured with a Bartington MS2E point sensor in a 4 mm interval over the whole core. That contrast can be used to determine the sediment transportation processes and where the sediments were found in Kjøsnestjorden. Organic material has a lower magnetic susceptibility than minerogenic materials. Within minerogenic materials, samples with more magnetic minerals as magnetite or hematite, have a higher MS number than minerals such as quartz.

### 3.2.4. Loss on Ignition (LOI)

The loss-on-ignition method can find the organic content in a lacustrine sediment sample. It was first used by Dean (1974).

During this survey, the sampling was done by measuring 1 cm<sup>3</sup> of sediment with a measuring syringe every 5 centimetres throughout the core. That sample was put into a crucible and dried in an oven at 105 °C for 24 hours to remove the water. The samples were weighed before and after drying (Dean, 1974). It is important to touch only with tweezers to prevent contamination by other materials, which could change the result. This concluded in 54 samples from core 603-21 01 PC and 49 samples from core 603-21 08 PC.

Then, the crucibles are put into a different oven and burned at 550 °C for an hour to remove any organic matter in the samples. After cooling down, they get weighed again, and the organic content is calculated (Dean, 1974).

The measured organic content can be an inverse indicator for glacial activity and sediment input (Karlén & Denton, 1976).

The results of the LOI analysis were also used to determine the best sampling spots for radiocarbon dating.

### 3.2.5. CT-scanning

In Earthlab at the University of Bergen, the ProCon X-Ray CT-ALPHA Computed Tomography (CT) scanner is utilized to measure the variations in density within sediment cores in a non-destructive manner (Orsi et al., 1994). This technique involves a fixed X-ray source that emits radiation, which is absorbed and scattered by the sediment sample before being detected by a stationary sensor. The CT scanner has a high degree of precision and produces data with exceptional resolution, enabling the identification of different grain sizes and shapes. The sediment core is positioned in the CT scanner and revolves through the X-ray beam (Støren et al., 2010). The results are processed and visualized using the FEI Avizo 3D software.

Core 603-21 01 PC (both parts) was scanned with a voltage of 125 kV, an electric current of 850  $\mu$ A, an exposure time of 334 ms and a 0,5 mm copper filter, taking 2400 projections per rotation.

Core 603-21 08 PC (part 2/2) was scanned with a voltage of 125 kV, an electric current of 850  $\mu$ A, an exposure time of 334 ms and a 0,5 mm copper filter, taking 1600 projections per rotation.

## 3.3. Dating Methods

### 3.3.1. Radiocarbon-Dating ( $^{14}\text{C}$ )

The samples were measured with an AMS (Accelerator mass spectrometry). The method is based on the element carbon having three naturally occurring isotopes: C12, C13 and C14. The first two are stable, and the latter is unstable. During a living 'organism's life, the three carbon

isotopes are in equilibrium. As soon as the organism dies, the C14, which has a half-life of 5730 years, starts to decay (Olsson, 1968)

To avoid the reservoir and hard water effects, macrofossils of terrestrial origin have been taken. Leaves and other fragile fossils are preferred to give a more accurate analysis result. Wooden sticks and barks can lie over decades on the lake floor without significant composting (Birks, 2007).

AMS counts the number of C14 atoms in the sample based on its specific atomic mass.

For the radiocarbon dates to be precise and accurate, it is important also to measure the stable isotopes. Then, the ratio between is used to determine the correct isotope fractionation as it takes place in nature.

Table 3 provides information about the samples taken for AMS-dating from core 603-21 01

<b>ID</b>	<b>Core, section</b>	<b>Sampling position</b>	<b>Sample type</b>	<b>Sample weight</b>
Poz-148726	603-21 01 1/2	35 cm	plant macrofossil	4,9 mg
Poz-148725	603-21 01 1/2	75 cm	plant macrofossil	4,6 mg
Poz-148723	603-21 01 1/2	112 cm	plant macrofossil	5,3 mg
Poz-148722	603-21 01 2/2	200 cm	plant macrofossil	4,3 mg
Poz-148786	603-21 01 2/2	240 cm	plant macrofossil	2,5 mg

Table 4 gives information about the samples taken for AMS-dating from core 603-21 08 PC

<b>ID</b>	<b>Core, section</b>	<b>Sampling position</b>	<b>Sample type</b>	<b>Sample weight</b>
Poz-149328	603-21 08 1/2	25 cm	bulk	10,4167 g
Poz-149324	603-21 08 1/2	50 cm	bulk	10,9613 g
Poz-149363	603-21 08 1/2	85 cm	bulk	12,3597 g
Poz-149323	603-21 08 1/2	122 cm	bulk	6,5647 g
Poz-149322	603-21 08 2/2	143 cm	bulk	4,9693 g

Poz-148727	603-21 08 2/2	170 cm	plant macrofossil	3,6 mg
Poz-148726	603-21 08 2/2	174 cm	plant macrofossil	5,8 mg

---

The chosen samples (see Table 3 and Table 4) were sent to the Poznan Radiocarbon Laboratory, at Adam Mickiewicz University.

### 3.3.2. Age-depth-model

To say something about how the various events related to glacial activity and climatic shifts, it's necessary to establish a realistic age chronology (Blaauw, 2010). The two sampling sites are quite different regarding sedimentation rate and proximity to the steep slopes surrounding Kjøsnestjorden.

An age-depth model with and without corrections for the event layers is constructed using the Bayesian framework in RStudio (Version RStudio 2022.07.1) with the rbacon Library (Version 2.5.8). The corresponding table with the measured dates was created in Microsoft Excel 365 and saved as a .csv-file (comma separated values) to be accessed by RStudio.

The calibration curve for terrestrial material in the Northern Hemisphere used was intCal20 (Reimer et al., 2016).

## 3.4. Data Analysis

### 3.4.1. Principal Component Analysis – PCA

Principal Component Analysis (PCA) is a method which makes it possible to show a relationship between measured parameters. It was performed in R, using RStudio (Version 2022.07.2, Build 576) by using various packages: dplyr, tidyr, rxtras, readxl, ggpubr, stats, ggfortify and an individual code script.

These can be chemical elements, magnetic susceptibility, and their reaction to various mechanisms. This study will be applied to core 603-21-08 PC to determine, which variables can be used to distinguish sediment units.

Vasskog et al. (2011), Bakke et al. (2013), Wittmeier et al. (2015) and Hardeng et al. (2022) have applied PCA to a large multivariate dataset, analysed sediment cores to identify the influence of different sediment sources and processes and isolated the glacially transported sediments. The following normalized results of the XRF-analysis: "inc/coh", K, Ti, Fe, Ca, Rb and Si as well as the MS value will be used to perform the PCA.

## 4. Results

### 4.1. Results of the field methods

#### 4.1.1. Bathymetric map and seismic survey

During the field course "GEOV226 – Field and Laboratory course in Quaternary Geology" in autumn 2021, a total of nine sediment cores (four piston cores and five gravity cores) were taken. In addition to the bathymetric survey presented in this chapter, four CHIRP profiles are also presented in this thesis.

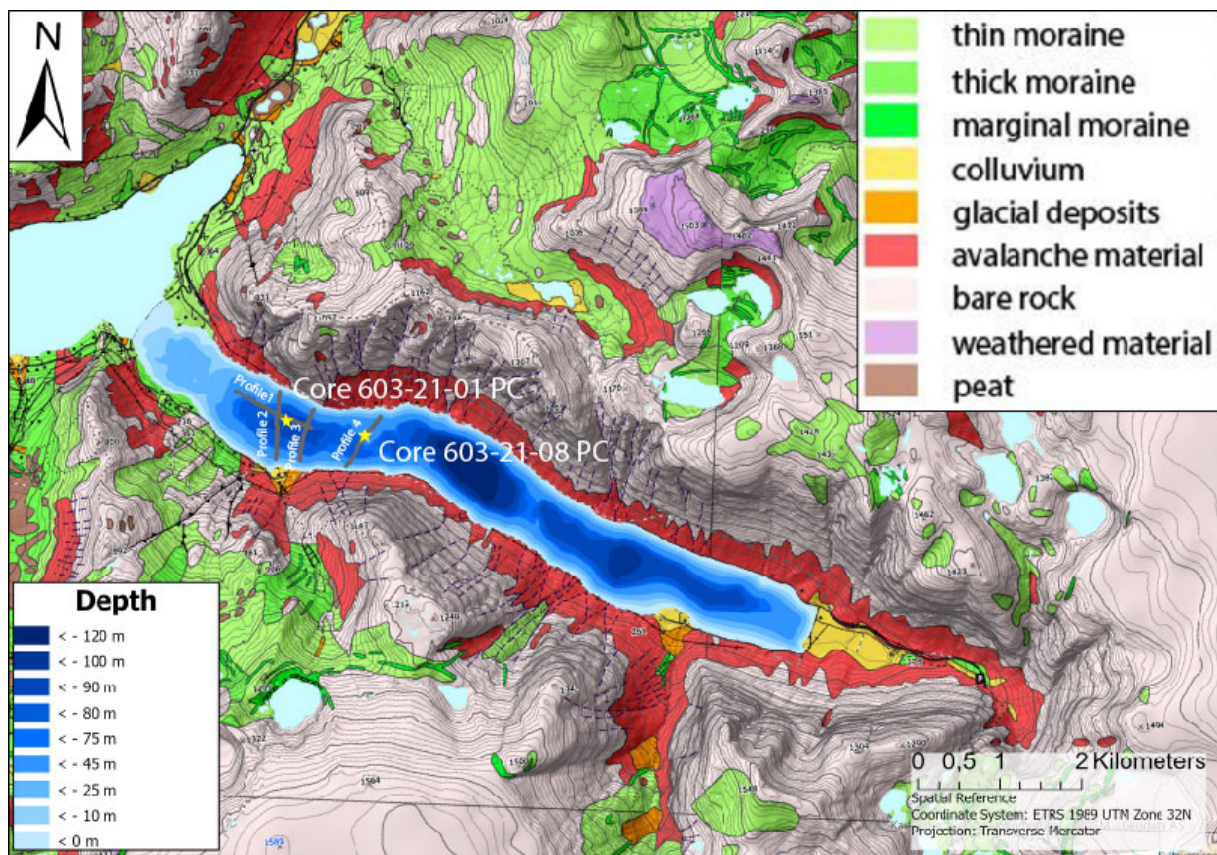


Figure 16 shows the bathymetric map of Kjøsnestjorden made in ArcGIS Pro with the “Topo to raster” interpolation and basic settings. It was then combined with the quaternary map from chapter 2 to highlight here the major inlets, which can be recognized with colluvium and glacial deposits. It also shows the locations of core 603-21-01 PC, core 603-21-08 PC and the CHIRP profiles 1 – 4.

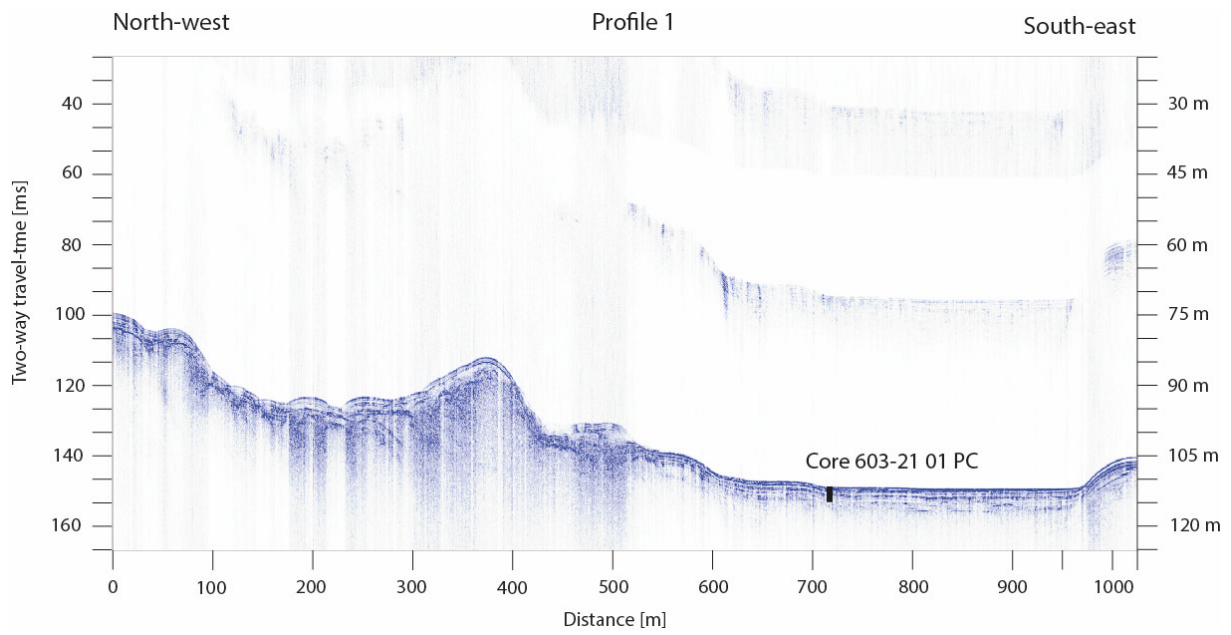


Figure 17 CHIRP profile 1 and the location of sediment core 603-21-01 PC on the lake floor.

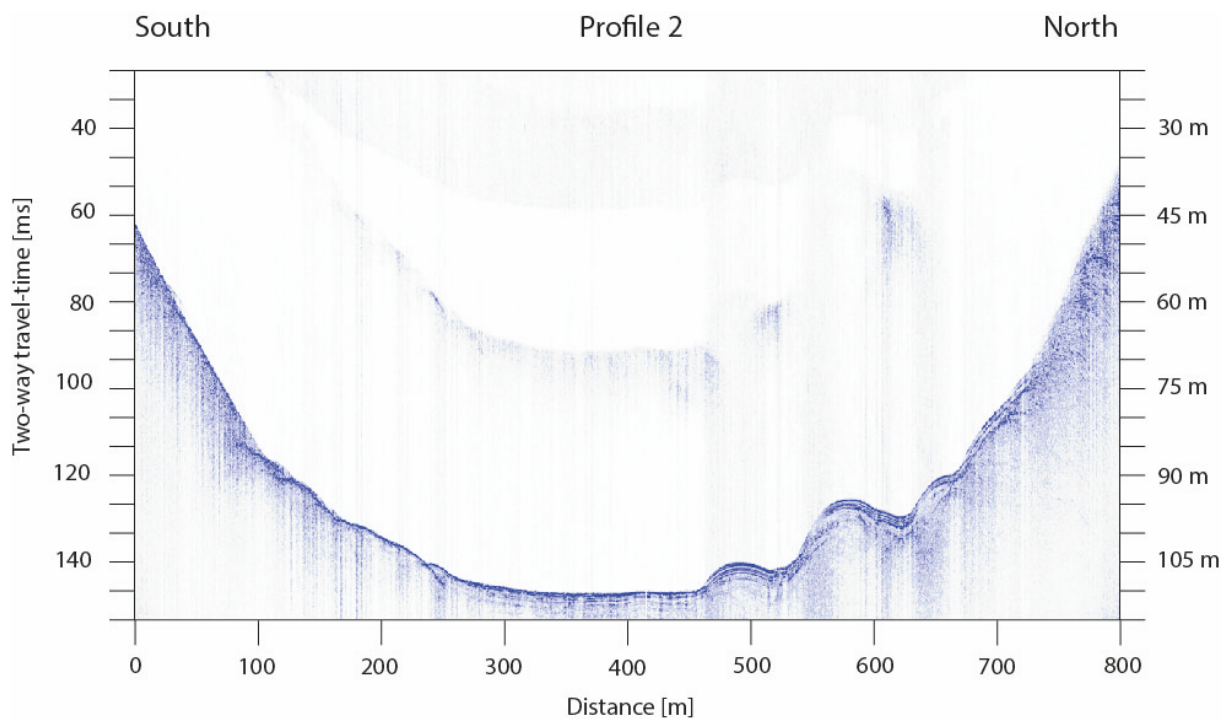


Figure 18 CHIRP profile 2 how the typical cross profile of the lake with steep slopes continuing from land and into the lake and soft sediments deposited in the central basin.

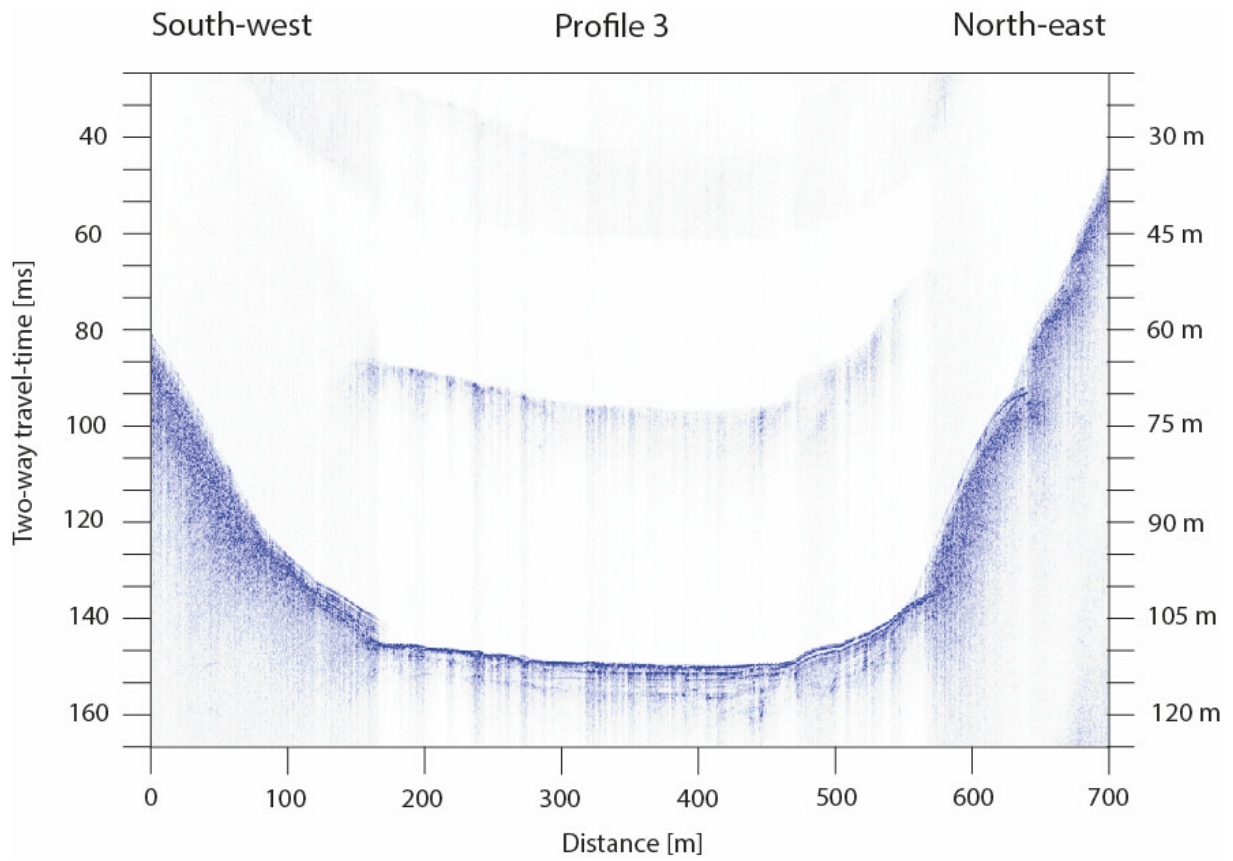


Figure 19 CHIRP profile 3, also a cross profile showing the undisturbed soft sediment package in the middle of the lake.



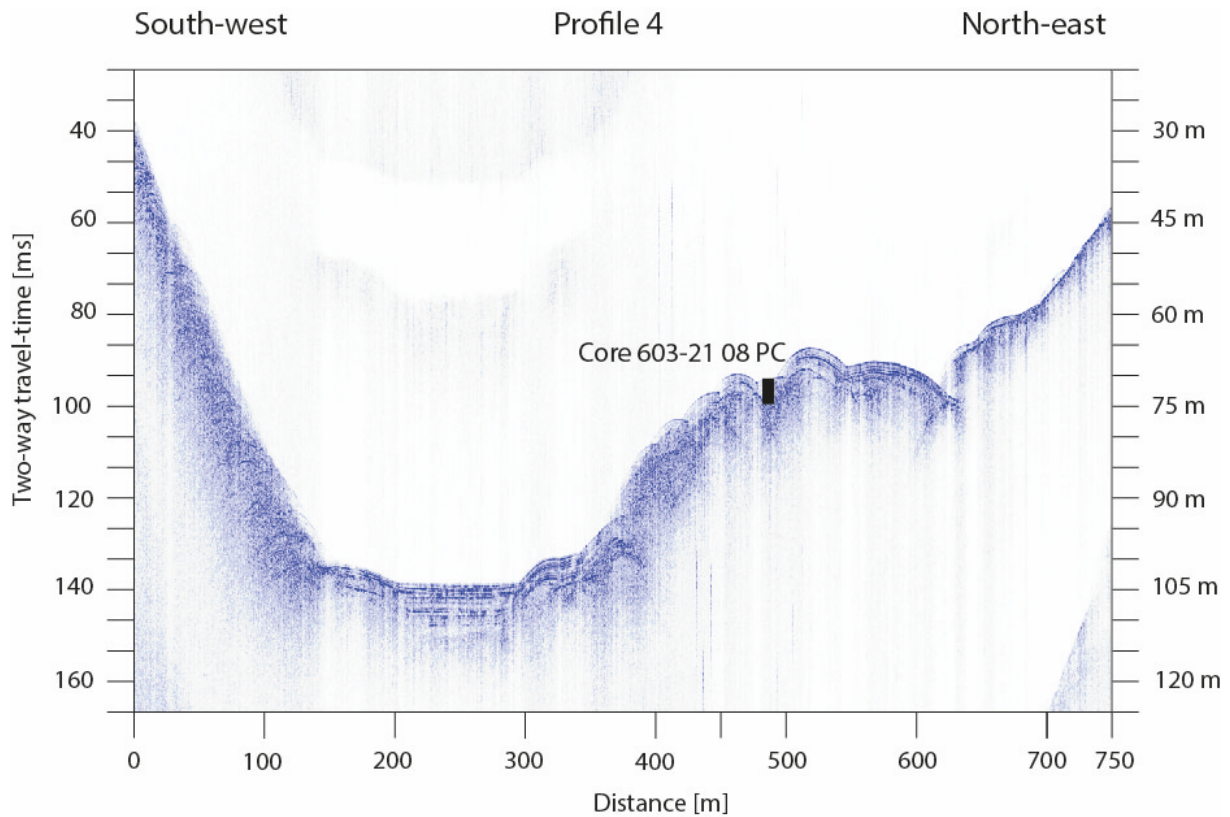


Figure 20 CHIRP profile four and the location of core 603-21-08 PC on the rise protected from the slope by a trench.

The bathymetric map (Figure 16) in combination with the CHIRP profiles (Figure 17, Figure 18, Figure 19 and Figure 20) shows that the lake consists of three basins with two thresholds within the lake and one on the North-west on the margin to Jølstravatnet. The CHIRP profiles and the map show that the steep slopes on shore continue in the lake. The lake itself is quite flat and the profiles show sediment thicknesses of a few meters. The coring position of core 603-21-01 PC is shown on profile 1 (see Figure 17) and was taken at a depth of 112 meters on the lake floor. Core 603-21-08 PC's exact coring position is shown on profile 4 (see Figure 20) at a depth of 70 meters. It's taken on the lake's slope next to a ridge. Profile 2 (see Figure 18), directing North-South, and profile 3 (see Figure 19), from south-west to north-east, both show the inlet slope from Sægrov, the relative flat lake floor and the opposing one, which is the steeper one.

## 4.2. Age model

### 4.2.1. Radiocarbon dating results

The results of the LOI analysis were used to determine the best sampling spots (with high organic content) for radiocarbon dating. This was applied for both the plant macrofossil picking as well as bulk sampling. Each sample contained enough organic material to be dated.

Due to measurement errors during the LOI analysis, the results in core 603-21-01 PC from 20 to 60 cm depth cannot be used. Instead, the samples were taken from organic-rich layers when viewed with the naked eye.

### 4.2.2. Core 603-21 01 PC

Table 5 shows the radiocarbon ages from core 603-21 01 PC and the calibrated ages with a 95% confidence interval, which were calculated by using RBAcon and the IntCal20 calibration curve.

ID	Core, Section	Depth	Sample material	C-14 age (yrs. BP)	1 s cal. age (yrs. BP)
Poz-148726	603-21 01 1/2	35 cm	plant macrofossil	250 ± 30	97 – 213
Poz-148725	603-21 01 1/2	75 cm	plant macrofossil	730 ± 30	247 – 400
Poz-148723	603-21 01 1/2	112 cm	plant macrofossil	340 ± 35	403 – 531
Poz-148722	603-21 01 2/2	200 cm	plant macrofossil	4235 ± 35	914 – 1197
Poz-148786	603-21 01 2/2	240 cm	plant macrofossil	1485 ± 35	1198 – 1405

### 4.2.3. Core 603-21 08 PC

A chronology has been done for the sediment record based on Accelerator Mass Spectrometry (AMS) radiocarbon dating of picked plant macrofossils and bulk sediment samples (see table 7).

Table 6 shows the radiocarbon dates from core 603-21 08 PC. The conventional dates were determined by the Poznan Laboratory and the calibrated ages were calculated by using RBAcon and the IntCal20 calibration curve.

ID	Core, Section	Position	Sample	Conventional C-14 age (yrs. BP)	Calibrated Age (yrs. BP)
Poz-149328	603-21 08 1/2	25 cm	bulk	775 ± 30	641 – 788
Poz-149324	603-21 08 1/2	50 cm	bulk	1525 ± 30	1318 – 1524
Poz-149363	603-21 08 1/2	85 cm	bulk	2775 ± 30	2767 – 2964
Poz-149323	603-21 08 1/2	122 cm	bulk	3355 ± 35	3492 – 3823
Poz-149322	603-21 08 2/2	143 cm	bulk	4205 ± 40	4541 – 4870
Poz-148727	603-21 08 2/2	170 cm	plant macrofossil	6980 ± 40	6872 – 7837
Poz-148726	603-21 08 2/2	174 cm	plant macrofossil	6390 ± 40	7182 – 7954

### 4.3. Age-depth model

The bacon age-depth-modelling with the IntCal 20 calibration curve was used to construct the age-depth models.

#### 4.3.1. Core 603-21 01 PC

For modelling this age-depth-curve, the radiocarbon ages from the samples of 35 cm, 112 cm and 240 cm (seeTable 5) were chosen. The other two samples display too old ages probably due to dating of older reworked macrofossil, which seems plausible given that the lake's slope is quite steep.

The blue lines show the calibrated age with one sigma up and down.

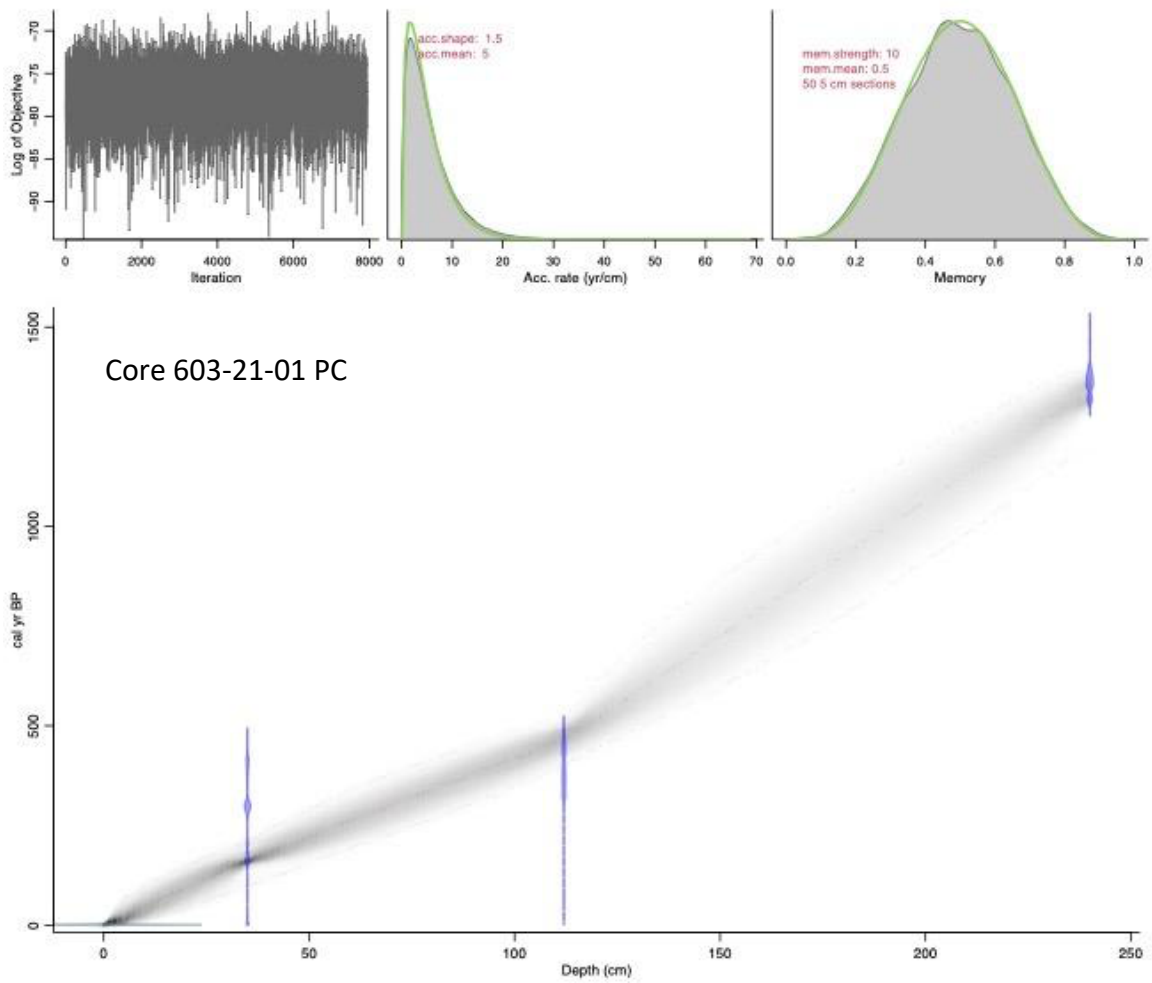


Figure 21 Age-depth-model of core 603-21 01 PC, created by the RBacon code using the calibrated radiocarbon ages from the depths 35 cm, 112 cm and 240 cm.

### 4.3.2. Core 603-21-08 PC

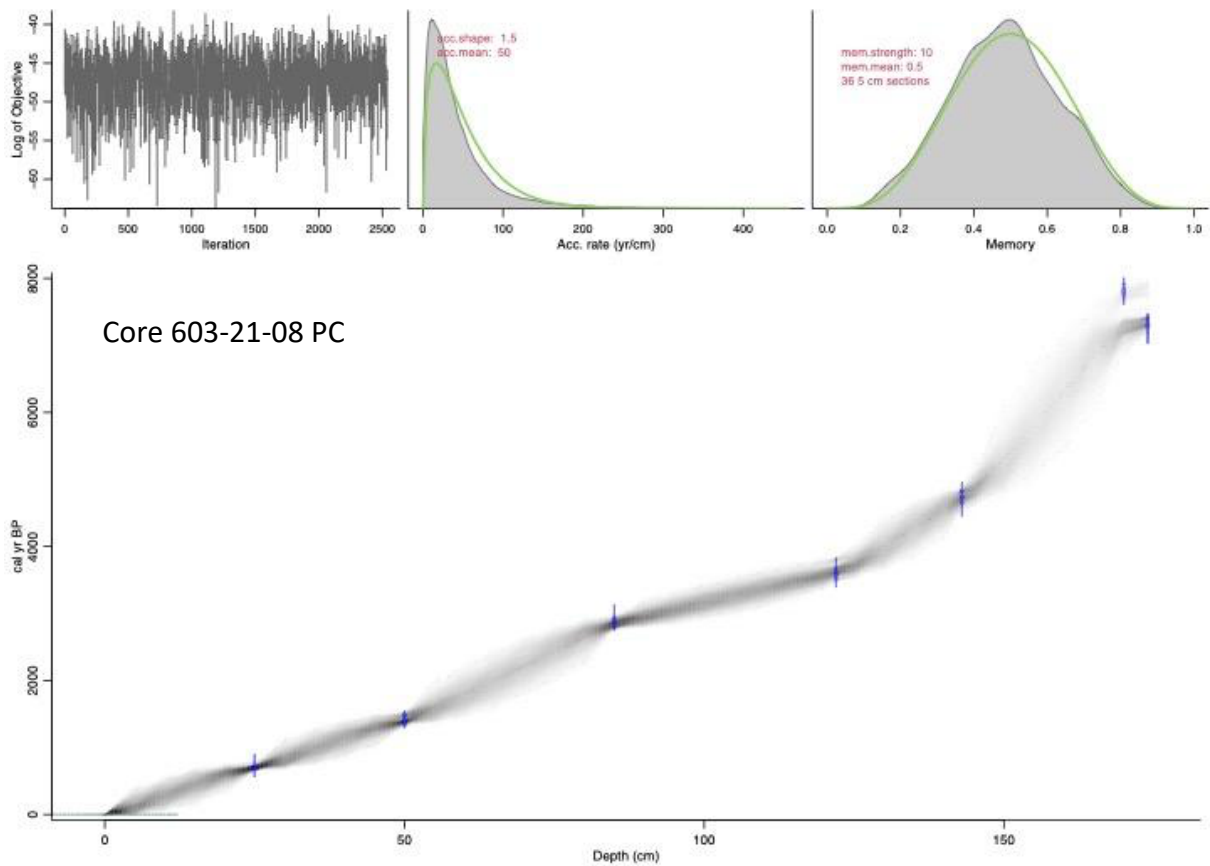


Figure 22 shows the age-depth curve of core 603-21-08 PC. It was created in RStudio with the RBacon package using the IntCal20 calibration curve (Reimer et al., 2020).

A total of seven samples have been used to calculate this age-depth curve. The blue lines show the calibrated age with one sigma up and down. The oldest calculated (and calibrated with the IntCal20 curve) age is 8000 cal. yrs. BP at a depth of 170 cm. According to the C-14 age and calibration results, the sample taken at 174 cm is younger than that taken at 170 cm.

## 4.4. Results of the sediment analysis

### 4.4.1. Description of core 603-21 01 PC

The layers in Core 603-21 01 PC have been categorised in five different facies according to visual properties and the manual log analysis.

Table 7 Overview of the units in core 603-21 01 PC and which optical properties were used to differentiate and categorize them. It also shows the colors, which are used in the plot.

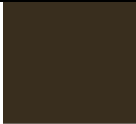
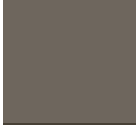


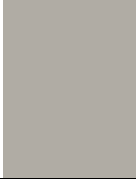
<b>Facies</b>	<b>Property 1</b>	<b>Property 2</b>	<b>Property 3</b>	<b>Color</b>	
A	Gyttja	Organic pieces	Fining upwards	Munsell 5y 2/2	
B	Sand	Fining upwards	Fine/medium/coarse	Munsell 5y 4/1	
C	Silt	Organics		Munsell 5y 3/1	
D	Silt	No organics		Munsell 5y 4/2	
E	Clay	Organics / No Organics	Lamination	Munsell 5y 7/0,5	

Table 8 Description of each interval in the sediment cores. The results are based on facies, sediment type and colour.

Facies	from	to	thickness [cm]	Sediment type (grain size)	Coulour	Description
C	0	2	2	silt	5y 3/1	fine grain small top layer
B	2	11,5	9,5	sand	5y 4/1	fine sand (larger than upper layer)
E	11,5	19	7,5	clay	5y 7/0,5	
B	19	26,5	7,5	sand	5y 4/1	fining upwards, organic material
E	26,5	33,5	7	clay	5y 7/0,5	Intercalation of clay and silt layers
A	33,5	37,5	4	gyttja	5y 2/2	gyttja
E	37,5	43	5,5	clay	5y 7/0,5	
B	43	45	2	sand	5y 4/1	
E	45	49	4	clay	5y 7/0,5	
D	49	51,5	2,5	silt	5y 4/2	
E	51,5	63,5	12	clay	5y 7/0,5	
B	63,5	66,5	3	sand	5y 4/1	medium sand
C	66,5	71,5	5	silt	5y 3/1	silt with organic
A	71,5	81	9,5	gyttja	5y 2/2	fining upwards of gyttja
C	81	86,5	5,5	silt	5y 3/1	silt with organic material

E	86,5	92	5,5	clay	5y 7/0,5	clay with little bit organic, lamination visible
B	92	103,5	11,5	sand	5y 4/1	fining upwards, lighter sediments bottom, larger sediments on top, colours: dark brown to grey to yellow
E	103,5	109	5,5	clay	5y 7/0,5	sharp transition to sand layer
A	109	112	3	gyttja	5y 2/2	small organic pieces
B	112	116	4	sand	5y 4/1	fine grained sand; organic material
E	116	124	8	clay	5y 7/0,5	Laminated clay with organic material
B	124	134,5	10,5	sand	5y 4/1	fining upwards sand sequence with organic material in the upper section
E	134,5	149	14,5	clay/silt	5y 7/0,5	laminated layers; clay and silt changing
D	149	156,5	7,5	silt	5y 4/2	mainly silt; one distinct silt lamination; bottom slightly more brownish tone
C	156,5	158,5	2	silt	5y 3/1	
E	158,5	163,5	5	clay	5y 7/0,5	laminated clay; organic layer
C	163,5	169,5	6	silt	5y 3/1	silt with organic material; little crack in layer
B	169,5	172,5	3	sand	5y 4/1	
E	172,5	179	6,5	clay	5y 7/0,5	sand; distinct crack in the upper part of this layer
D	179	183,5	4,5	silt	5y 4/2	fine silt
C	183,5	189,5	6	silt/gyttja	5y 3/1	slightly cracked silt with many wood/branch pieces in between; slightly cracked silt layer with many wood/branch pieces in between
B	189,5	194,5	5	sand	5y 4/1	fining upwards; lighter greyish color in bottom -> getting darker on top
E	194,5	199,5	5	clay	5y 7/0,5	very homogenous clay; big piece of wood



C	199,5	202,5	3	silt	5y 3/1	silty layer (fine silt) with organic matter
E	202,5	211,5	9	clay	5y 7/0,5	mostly homogenous clay with few tiny cracks
B	211,5	215	3,5	sand	5y 4/1	silty sand; organic matter
E	215	218	3	clay	5y 7/0,5	
C	218	220,5	2,5	silt	5y 3/1	silt with organic material
E	220,5	224	3,5	clay	5y 7/0,5	clay with few small cracks
D	224	227	3	silt	5y 4/2	very fine silt
E	227	230,5	3,5	clay	5y 7/0,5	clay (more grey/greenish compared to below)
D	230,5	235	4,5	silt	5y 4/2	silt
C	235	251	16	silt	5y 3/1	mostly homogenous silt with organic
B	251	264,5	13,5	sand	5y 4/1	fining upwards, sand layer, slightly brighter color in upper part-> darker in the bottom, clay patches

---

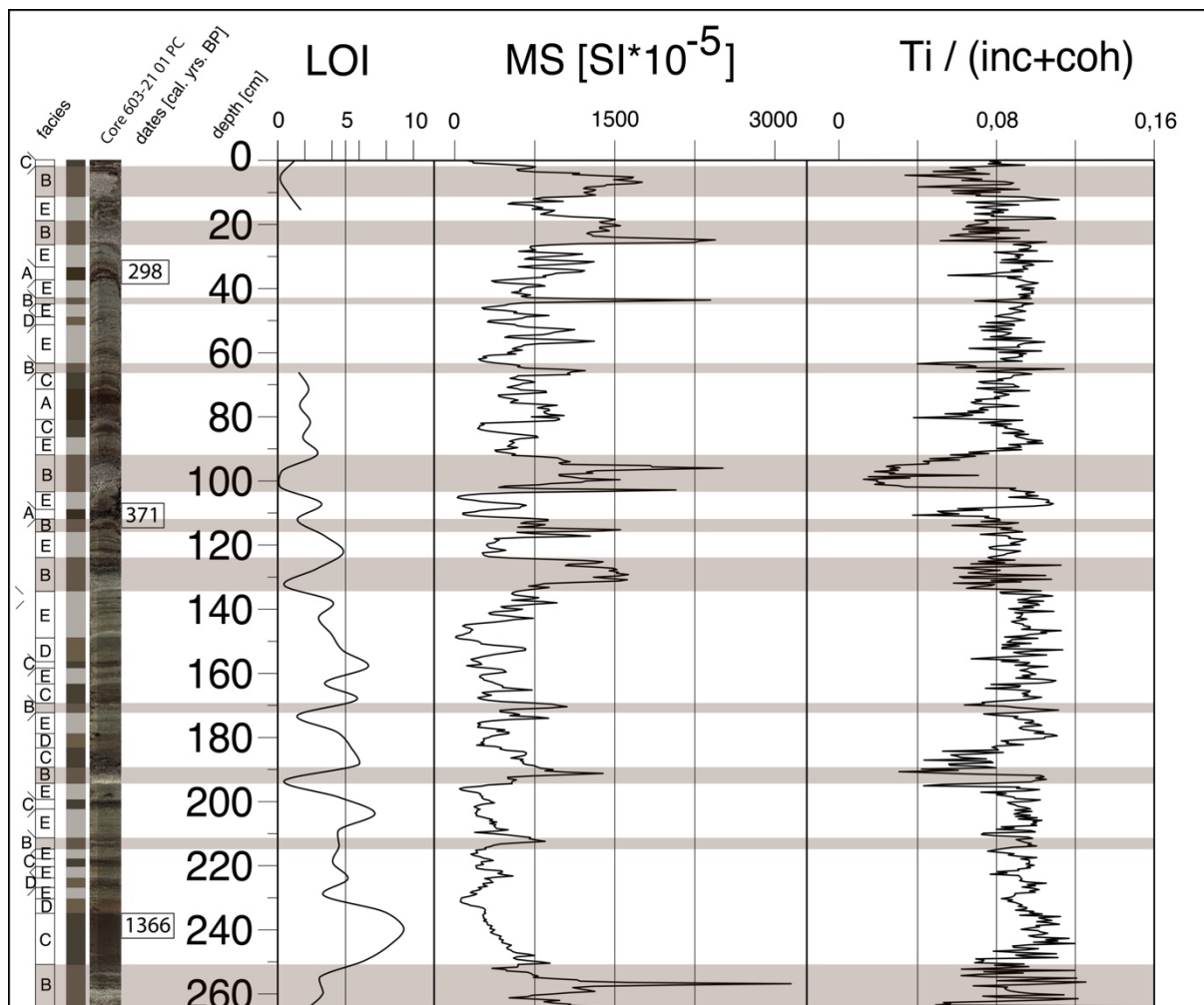


Figure 23 Overview of core 603-21 01 PC. It shows the categorized units, a scan of the core, the calibrated radiocarbon ages, the LOI values, the MS-values, and the Ti/(inc+coh)-ratio.

Figure 23 shows a scan of core 603-21 01 PC, as well as the categorized facies. It also shows the plots of the measured MS, the Ti/(inc+coh) XRF-data. The measurements have been divided by (inc+coh) to remove scatter effects (Kylander et al., 2011).

### Description of the facies:

#### **Facies A:**

Facies A (see Figure 24) consists of gyttja (color: 5y3/1 on the Munsell color chart). From 71,5 to 81 cm, a fining upwards trend is visible. The MS values range from 76 to 1217, and the mean value is 708 MS<sup>-10</sup>.

The Ti/(inc+coh) values vary from 0.037 to 0,097, whereas the lower values represent spikes.

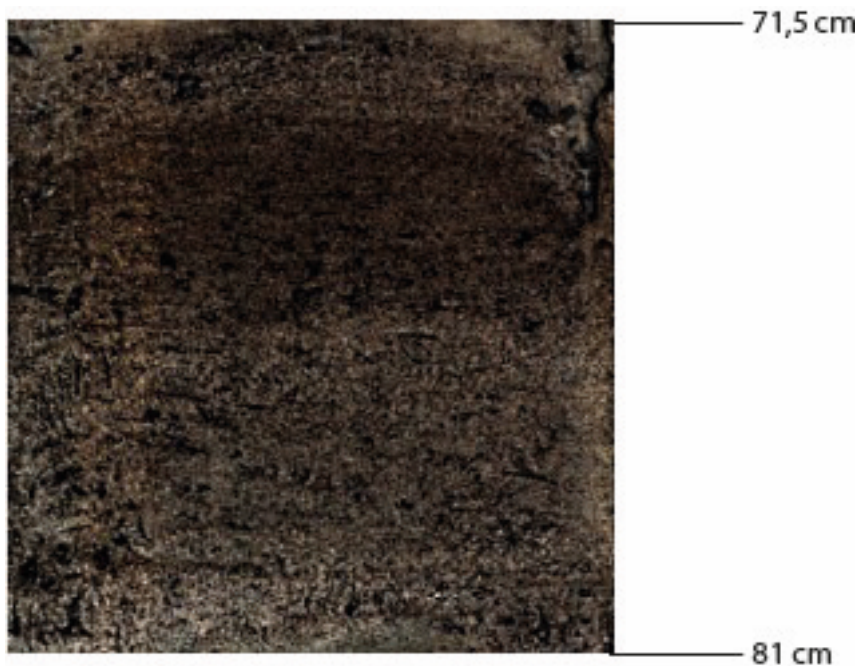


Figure 24 This section from core 603-21 01 (from 71,5 to 81 cm) shows the typical lithology found in unit A: gyttja with a fining upwards trend.

#### **Facies B:**

Facies B consists of sand (colour 5y4/1 on the Munsell colour chart), including fining-upwards sequences (see Figure 25). The sand can also contain organic matter. The MS values range from 196 to 3153. There are spikes at 24,8 cm (MS=2442), 43,6 cm (MS=2397), 96 cm (MS=2513), 03,2 cm (MS=1462), 115,2 cm (MS=1553), 129,2 (MS=1627), 130,8 cm (MS=1618), 170,4 cm (MS=1052), 191,2 cm (MS=1390) and the biggest one at 256,8 cm (MS=3153). The mean value is 1074.

The normalized Ti values range from 0,013 to 0,15. Fluctuating values can be observed from 2,4 to 11,6 cm. From 92,4 to 101,2 cm, the values decrease from 0,69 to 0,018. There is a

negative spike at 190,4 cm with a value of 0,0305. From 251,6 to 264,4 cm, the values show spikes in both directions: 0,05 at 263,6 cm and 0,152 at 264 cm.

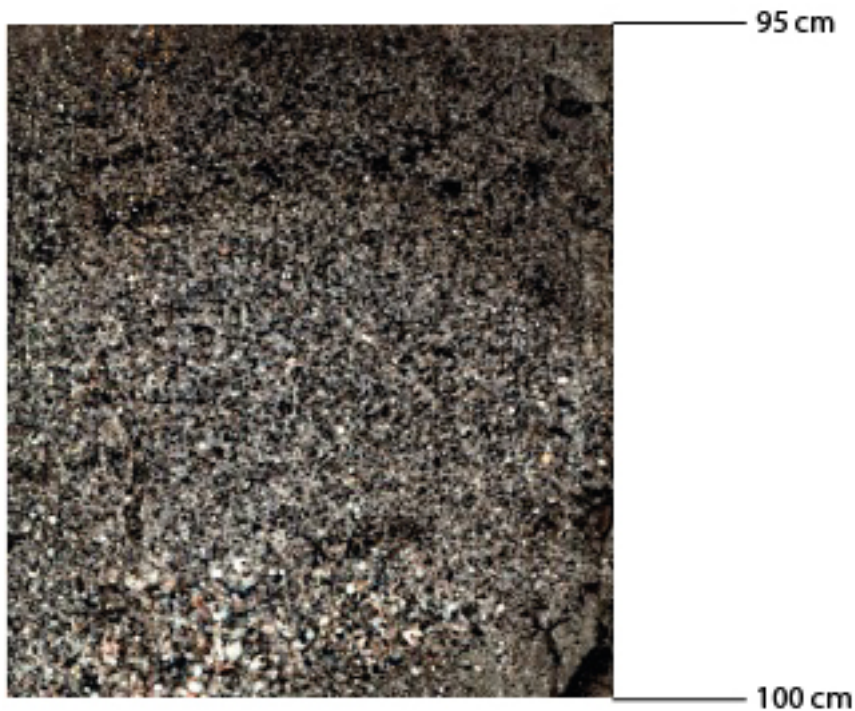


Figure 25: This section from core 603-21 01 (from 92 to 104 cm) shows a fining upwards sequence of coarse to medium-grained sand, which can also be found in unit B.

### **Facies C:**

Facies C (see Figure 26) consists of silt in combination with organic material in colours 5y 3/1 on the Munsell colour chart. The MS values are 8 to 1270. From 235,2 to 250,4 cm, the MS values increase from 266 to 893. The mean value is 433.

The normalized Ti values range from 0,043 to 0,12. There are negative spikes at 82 cm with a normalized Ti value of 0,071 and at 187,2 with a value of 0,043.



Figure 26: This section from core 603-21 01 (from 199,5 to 202,5 cm) shows the typical lithology found in unit C: fine silt with organic matter.

#### **Facies D:**

Facies D (see Figure 27) consists of organic-free silt in color 5y 4/2 in the Munsell color chart. In the upper part of the core, there is intercalation of clay and silt layers. The MS values vary from 53 to 1076. The mean value is 350.

The normalized Ti values range from 0,067 to 0,113.

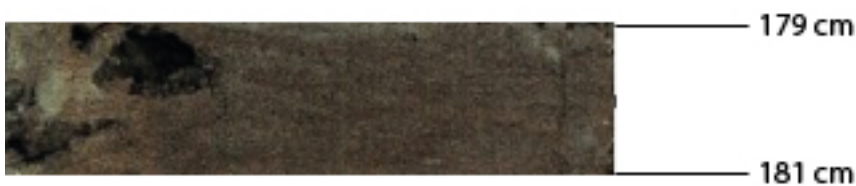


Figure 27: This section from core 603-21 01 (from 179 to 181 cm) shows the typical lithology found in unit D: organic free fine silt.

#### **Facies E:**

Unit E consists of clay, often containing organic material (see Figure 28) as well as laminations in color 5y4/2 and 5y3/2 on the Munsell color chart. The MS values range from 15 to 1504. The mean is 511.

There are several spikes in the top half of the core at 18,4 cm (MS=1504), 31,6 cm (MS=1306) and 56,4 cm (MS=1308).

The normalized Ti values range from 0,04 to 0,113. There are spikes at 12,4 cm (Ti = 0,11), 18,4 cm (Ti = 0,11), 140,8 cm (Ti = 0,109), 146,8 cm (Ti = 0,113) and at 162,4 cm (Ti = 0,11).



Figure 28: This section from core 603-21 01 (from 202,5 to 212 cm) shows the typical lithology found in unit F: laminated clay with organic matter.

Event intervals:

The event intervals are picked on positions where they show a spike or an easy distinguishable pattern in the grain counts.

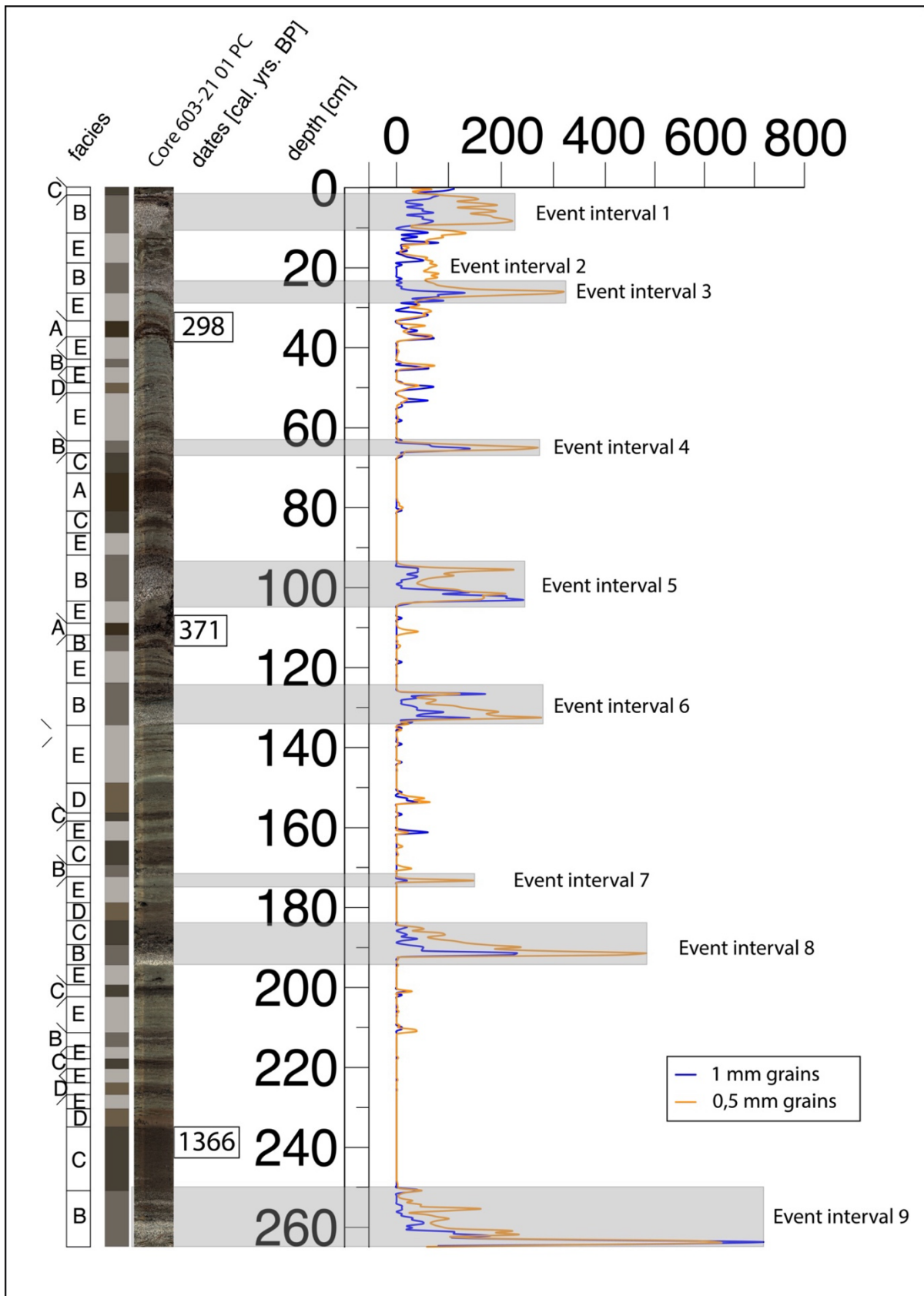


Figure 29 shows the grain counts (0,5 mm and 1 mm) performed with the FEI Avizo 3D software next to the categorized units and a image of core 603-21-01 PC. The 1 mm grain counts have been multiplied by 10 for a better visualization.

Event interval 1: 1 to 11 cm

Event interval 1 is within facies B, shows a MS spike with values of up to 1700 and normalized Ti values from 0,035 to 0,09.

Event interval 2: 17 to 22 cm

Event interval 2 consist of a turbulent (see core image) facies E and facies B with lower MS values (500) at the beginning and higher values at the end (1500). The normalized Ti values show a spike at 18 cm of 1,1.

Event interval 3: 22 to 29 cm

Event interval 3 consists of facies B (top) and E (bottom). It shows a clear spike in the grain counts, which fits with a MS spike with a value of 2400. The normalized Ti values range from 0,065 to 0,1.

Event interval 4: 62 – 66 cm

Event interval 4 presents a grain count spike in facies B, which shows a MS spike with values up to 1000. The normalized Ti values also show a spike and values up to 0,115.

Event interval 5: 93 to 105 cm

A fining upwards sequence here is followed by a spike in facies B. The MS values show two spikes. The lower has a value of 2100 while the upper has a value of 2500. The normalized Ti values show negative spikes with values from 0,02 to 0,07.

Event interval 6: 124 to 134 cm

A fining upwards sequence here is followed by a spike in facies B. The MS value spikes up to 1600, while the normalized Ti values vary from 0,06 to 0,095.

Event interval 7: 172 to 175 cm

A spike in unit E and B with significant more grains in the 0,5 mm size (representing small sand) than 1mm shows a MS spike at 1250 and a negative Ti (norm.) spike at 0,03.



Event interval 8: 183 – 194 cm

A fining upwards sequence in facies B (bottom) and C (top), shows a spike in the MS measurements at 1450 as well as both a positive and a negative spike in the Ti (norm) values at 0,11 and 0,03

Event interval 9: 250 to 264,5 cm

A huge spike in both grain size fractions and a smaller one (only in the 0,5 mm grains) results in facies B shows a MS spike at 3100 and Ti (norm.) values from 0,06 to 0,15.

#### 4.4.2. Description of core 603-21 08 PC

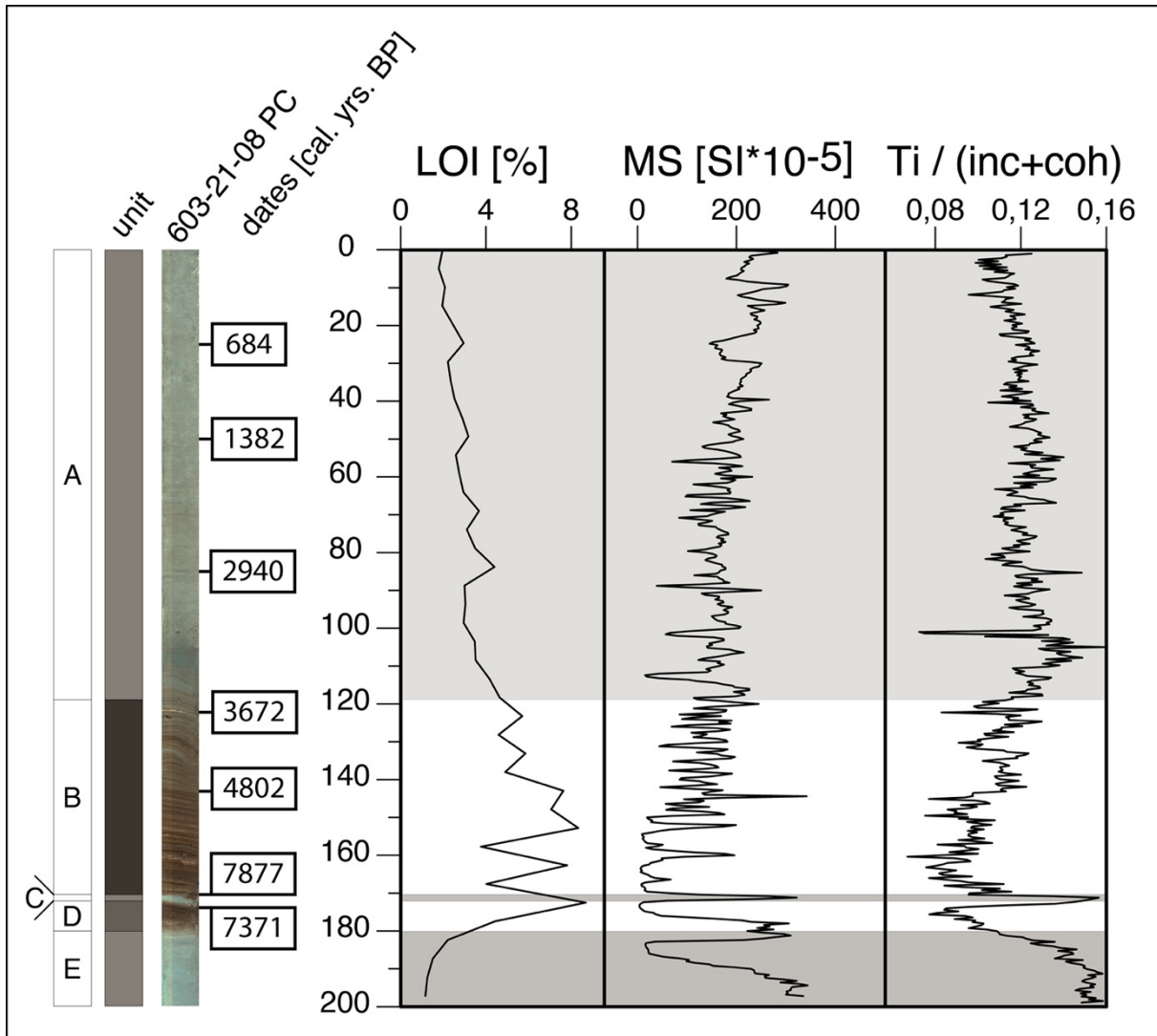


Figure 30 Over of core 603-21 08 PC with a core image, different units, calibrated ages, MS, LOI, DBD, Fe and Ti (both normalized by dividing it by (int+coh)).

After the core has been split, the layers in the cores were described cm by cm.

The units, which are described in the next paragraphs, were chosen based on visual appearance as well as on general trends in the MS and XRF analysis. The visualization of the data is limited to 200 cm length of this core, because we decided to not use it for the purpose of this project.

**Unit A: 603-21 08 PC 119,5 to 0 cm**

This unit's colour is 5y-4/1 from 119,5 to 114 cm. It changes to 5y-3/2 in the remaining layer. The MS values vary from 15 to 226. The LOI values are 3,52 % and 4,20 %. The DBD values are 0,64 g/cm<sup>3</sup> and 0,78 g/cm<sup>3</sup>. The normalised Fe values range from 1,25 to 2,58 and the Ti results vary from 0,037 to 0,11.

This unit becomes more clayey and has a dark grey colour (colour 5y-4/2 on the Munsell colour chart (Munsell & Color, 1951)) from 105,4 cm to 0 cm. The MS values range from 33 to 305 and increase towards the top of the core. The LOI results in a decrease towards the top of the core and has values from 1,79 % to 4,40 %. The DBD, inversely correlated with the LOI, increases from 0,538 to 0,823 g/cm<sup>3</sup>. The Fe values decrease towards the top of the core and range from 0,61 at 5,2 cm to 2,35 at 84 cm. The normalised Ti data varies from 0,033 to 0,11.

**Unit B: 603-21 08 PC 170,4 to 142,5 cm to 119,5 cm**

Facies D consists of gyttja and fine sand layers in brown colour (5y-2.5/1 in the Munsell chart). There are also layers with high organic content from 161,5 – 165 cm and a single clast (1 cm size) at 160 cm. The LOI results vary between 3,8 and 8,3 %. The DBD values vary between 0,42 g/cm<sup>3</sup> and 0,80 g/cm<sup>3</sup>. The Fe values have high variations ranging from 1,83 to 3,08. The Ti values range from 0,064 (170,0 cm) to 0,114 (152,8 cm).

This unit continues at 142,4 cm upwards with alternating gyttja and silt layers. brown-greyish color (color code 5y-3/1 in the Munsell chart ).

The organic content (layered with silt) increases from 128 to 124 cm. It is followed by a significant 1 cm thick grey silt layer from 122 to 123 cm. The grain size changes to be silt dominant at 119,5 cm. The MS values range from 44 (at 131,2 cm) to 190 (at 124,4 cm). The LOI values range from 4,6 % to 5,8 % and the DBD values vary from 0,59 g/cm<sup>3</sup> to 0,73 g/cm<sup>3</sup>. The normalized Fe values range from 0,86 to 2,75 and the normalized Ti values range from 0,0010 to 0,0071.

**Unit C: 603-21 08 PC 172,4 to 170,4 cm**

Unit E consists of light-grey silt (color 5y-5/1 Munsell chart value. There was no sample for LOI and DBD taken. The MS values in this unit range from 128 to 322. The normalized Fe values range from 2,00 to 2,81. The normalized Ti values range from 0,084 to 0,111.

**Unit D: 603-21 08 PC 180,2 to 172,4 cm**

Unit F consists of brown-colored gyttja (colour 5y-4/1 Munsell chart value).

The LOI value is 8,7 % at 175 cm. The DBD value is 0,51 g/cm<sup>3</sup>. The MS values decrease from 222 at 180 cm to 12 at 172,4 cm. The Fe values decrease from 64500 cps at 180 cm to 41200 cps at 172,8 cm. The Ti values decrease from 2400 cps at 180 cm to 1700 cps at 172,8 cm.

**Unit E: 603-21 08 PC 200 cm to 180,4 cm**

The bottom part of 603-21-08 PC is defined as unit G and consists of silt with layers of sand.

The LOI values increase from 1,2 % at 200 cm to 5 % at 180,2 cm. The DBD values decrease in the same interval from 1,16 g/cm<sup>3</sup> at 200 cm to 0,69 g/cm<sup>3</sup> at 180 cm. The LOI and DBD values are correlated inversely. The MS values are 496 at 199,6 cm and decrease to 16 at 183,6 cm before the increase to 251 at 180,4 cm.

The values of Fe and Ti behave similarly. The normalised Fe values range from 3,35 to 3,75.

The normalised Ti values vary from 0,122 to 0,163 over this unit.

## 4.5. Data Analysis

### 4.5.1. Principal Component Analysis – PCA

#### 4.5.1.1. Core 603-21-08 PC

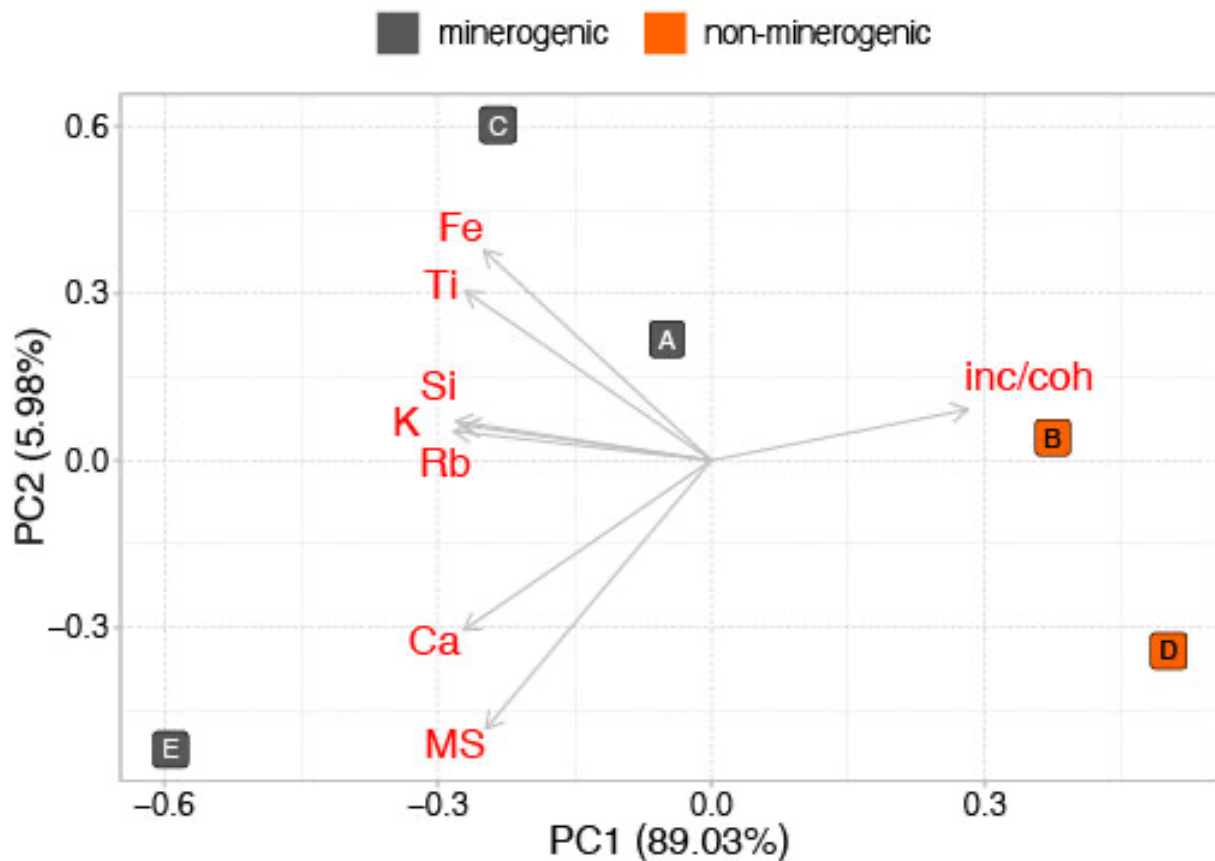


Figure 31 Biplot showing the result of a Principal Component Analysis (PCA) for the first (PC1) and the second Principal Component (PC2). The grey squares, display the minerogenic and the orange squares the non-minerogenic units of core 603-21-08 PC. The letters in the squares correspond to the respective unit from the sediment analysis. The XRF analysis and the MS results were averaged and used for this PCA: “inc/coh”, K, Ti, Fe, Ca, Rb and Si. The variable scores are displayed as vectors. The angle between two variables shows what type of correlation exists. A 90-degree angle shows virtually no correlation and a 0-/180-degree angle shows a very high positive/negative correlation.

The results of the PCA show a correlation between Fe and Ti as well as between Ca and the MS value. There is no correlation between the Fe and Ca and Ti and the MS value. A high positive correlation exists between K, Si and Rb and a high negative correlation between “inc/coh” and K, Rb and Si.

## 5. Discussion

The field work for this project was done during the GEOV226 field trip. This included bathymetric mapping, CHIRP surveys and coring. The results have already been presented in the last chapter.

For this project, the chosen cores 603-21-01 PC and 603-21-08 PC were analysed with the ITRAX XRF scanner, a CT scanner, the GEOTEK and LOI and grainsize measurements were performed in the EARTHLAB at the University of Bergen.

Although the sediments cores were taken in the same lake and analysed with the same methods, the interpretation can be completely different. For example: a high MS value can either be interpreted as an avalanche signal or as strong glacial activity.

While Core 603-21-01 PC is interpreted for avalanche deposits, core 603-21-08 PC is interpreted to show the glacial history of Jostedalbreen and Grovabreen. This means that the drawn conclusions will differ fundamentally.

### 5.1. Uncertainties

The ITRAX XRF scanner is a precise analytical instrument, it is therefore crucial to consider variables and uncertainties that come together with the analysis.

Measuring errors can occur, when the surface of the core has uneven bumps, gets dry or other factors can influence and decrease the accuracy of the analysis.

Before measuring, the core's surface has been carefully evened and a thin plastic film has been put on to avoid drying of the sediment surface during the measurements. Additionally, the software Q-Spec was used with the correct settings according to the instructions provided by the Earthlab.

The results of the XRF analysis must be regarded as semi-quantitative, which means that the reported output in “counts per second” (cps) are related to each other.

Also, the results are influenced by the water content and resulting density changes during the analysis. We were aware of occurring scattering effects and normalized the element counts by dividing it by the sum of “incoherent” plus “coherent” prior to further interpretation (Kylander et al., 2011).

## 5.2.Core 603-21-01 PC

### 5.2.1. Age-depth model

The established age-depth model is based on three of the five calibrated radiocarbon ages. The other two samples (Poz-148725 and Poz-148722) show older ages. The samples are hand-picked plant macrofossils and we assume that reworked older material was dated in both cases. During the picking, we tried to pick leaves and other short-lasting material, when available.

The material can also be contaminated by the sieving, picking and washing out macrofossils. Other uncertainties in the radiocarbon dating include changes in the Earth’s magnetic field, atomic bomb influence, solar activity variations in the atmosphere and human activities. This results in a reservoir effect, in which C-14 is broken down and new C-14 is not available. The calibration of radiocarbon dating is necessary to correct that, which is done by using calibration curves (Reimer et al., 2013).

We did consider the event layers while establishing the age-depth model. They are particles in between the normal sedimentation and there is also erosion from the events visible. Therefore, we concluded, that they don’t influence the overall sedimentation rate and the age-depth model.

### 5.2.2. The interpretation of different sediment signatures

#### Facies A:

We consider facies A to be background sedimentation of organic material, as it is contained in facies B, C and E as well, the only exception being facies D.

#### Facies B:

Facies B consists of highly minerogenic sand particles, that are often deposited in fining upwards sequences and can contain organic matter.

The steep slopes on land (see figure 1), which continue underwater (see figure bathymetric map and chirp profiles) provide the geomorphological environment and lead in combination with high precipitation and the westerlies (see chapter 2) to numerous snow avalanche events. Snow avalanches are high-energy events, which are capable of transporting rocks in various grainsizes down a slope (Blikra & Nemec, 1998). With decreasing energy, bigger pebbles and grains are deposited on land, while smaller fractions are transported further into the lake. Depending on a present ice will those be directly deposited on the lake floor or after the ice has melted.

Seierstad et al. (2001), Nesje et al. (2007), Vasskog et al. (2011) and Hesjedal (2022) present snow avalanche data from the Holocene, with increasing rates in the late Holocene (see figure XY).

The location of core 603-21-01 PC on the lake floor (see figure with chirp profile 1) is optimal to capture slope processes. Compared to core 603-21-08 PC and the determined calibrated ages, it features a longer sediment record in a shorter timespan, which also results in different average sediment accumulation rates (see figure 22 and 23; Core 603-21-01 PC: 5 yrs./cm vs. core 603-21-08 PC: 50 yrs./cm).

A grain count of particles greater than 0,5 mm and 1 mm has been performed and the results plotted on a depth scale (see figure counts vs. The highest counts occur in facies B.



All these facts lead to the conclusion that the sediments in facies B are deposited by snow avalanches. This concurs with Sabatier et al. (2022)'s interpretation.

Facies C:

We consider facies C to be also part of the background sedimentation, as it features unsorted silt with organic material.

Facies D:

We consider facies D, consisting of silt to be background sedimentation or of fluvial origin. Kjøsnesfjorden has rivers entering at Lunde, Sægrov and Sygnesand (see Figure 5) with their sediment load getting transported to the lake floor.

Facies E:

Facies E consists of laminated clay and organic matter. Kjøsnesfjorden being a glacial lake (see chapter 1), we assume that glacial flour (van der Bilt et al., 2015) originating from Jostedalsbreen and Grovabreen (see figure 2), transported by rivers entering the lake (see figure 5 with localities Lunde, Sægrov and Sygnesand) with their suspension load, where it gets disseminated and slowly falls to the lake bottom. There it can form laminations, when not being interrupted by events.

Table 8 shows the different facies, thicknesses, sediment types and the interpreted process for core 603-21-01 PC.

<b>Facies</b>	<b>from</b>	<b>to</b>	<b>thickness [cm]</b>	<b>Sediment type</b>	<b>process</b>
C	0	2	2	silt	background sedimentation
B	2	11,5	9,5	sand	snow avalanche
E	11,5	19	7,5	clay	glaciofluvial
B	19	26,5	7,5	sand	snow avalanche
E	26,5	33,5	7	clay	glaciofluvial
A	33,5	37,5	4	gyttja	background sedimentation
E	37,5	43	5,5	clay	glaciofluvial
B	43	45	2	sand	snow avalanche
E	45	49	4	clay	glaciofluvial
D	49	51,5	2,5	silt	Background / fluvial
E	51,5	63,5	12	clay	glaciofluvial
B	63,5	66,5	3	sand	snow avalanche
C	66,5	71,5	5	silt	background sedimentation
A	71,5	81	9,5	gyttja	background sedimentation
C	81	86,5	5,5	silt	background sedimentation
E	86,5	92	5,5	clay	glaciofluvial
B	92	103,5	11,5	sand	snow avalanche
E	103,5	109	5,5	clay	glaciofluvial
A	109	112	3	gyttja	background sedimentation
B	112	116	4	sand	snow avalanche
E	116	124	8	clay	glaciofluvial
B	124	134,5	10,5	sand	snow avalanche
E	134,5	149	14,5	clay/silt	glaciofluvial

D	149	156,5	7,5	silt	background / fluvial
C	156,5	158,5	2	silt	background sedimentation
E	158,5	163,5	5	clay	glaciofluvial
C	163,5	169,5	6	silt	background sedimentation
B	169,5	172,5	3	sand	snow avalanche
E	172,5	179	6,5	clay	glaciofluvial
D	179	183,5	4,5	silt	background / fluvial
C	183,5	189,5	6	silt/gyttja	background sedimentation
B	189,5	194,5	5	sand	snow avalanche
E	194,5	199,5	5	clay	glaciofluvial
C	199,5	202,5	3	silt	background sedimentation
E	202,5	211,5	9	clay	glaciofluvial
B	211,5	215	3,5	sand	snow avalanche
E	215	218	3	clay	glaciofluvial
C	218	220,5	2,5	silt	background sedimentation
E	220,5	224	3,5	clay	glaciofluvial
D	224	227	3	silt	background / fluvial
E	227	230,5	3,5	clay	glaciofluvial
D	230,5	235	4,5	silt	background / fluvial
C	235	251	16	silt	background sedimentation
B	251	264,5	13,5	sand	snow avalanche

### 5.2.3. Linking processes to event intervals:

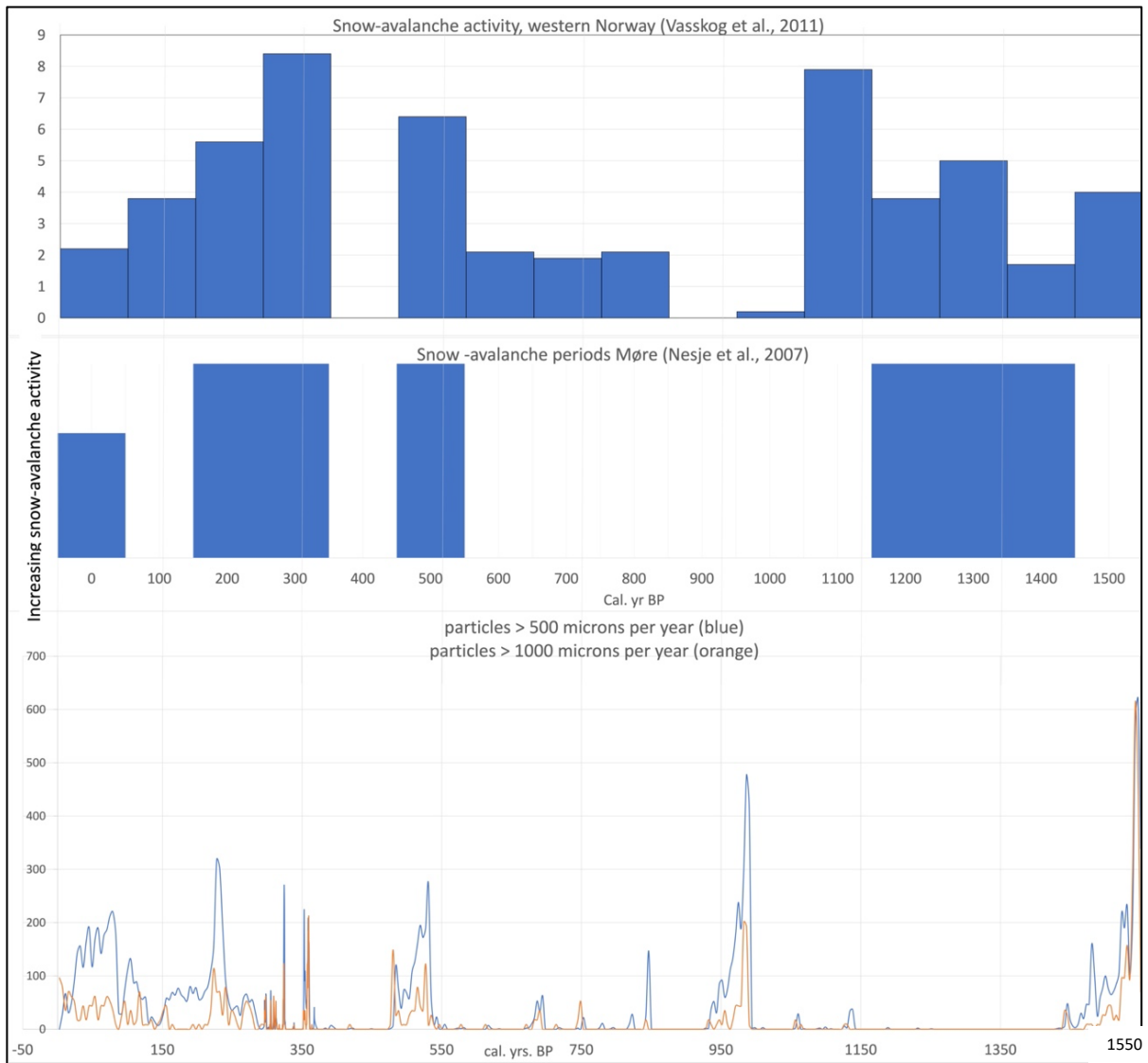


Figure 32 compares the grain counts (500 microns and 1000 microns) of core 603-21-01 with the avalanche frequency records of Nesje et al. (2007) and Vasskog et al. (2011).

Event interval 1: 20<sup>th</sup> century to present

Facies: B

Although, the Little Ice Age has ended in the late 19<sup>th</sup> century, the glacial activity and possible snow avalanches were still ongoing given that glaciers, such as Nigardsbreen, continued growing in the 1990s (Andreassen et al., 2020) as an of increased winter precipitation, higher glacier activity resulting in a positive NAO and therefore more avalanches.

Process: snow avalanche

Event interval 2: 250 to 150 yrs. BP

Facies: B and E

Nesje et al. (2007) and Vasskog et al. (2011) document increased snow avalanche activity, caused by increased glacier activity during the LIA, which lasted from the late 15<sup>th</sup> to the end of the 19<sup>th</sup> century (Nesje et al., 2000; Nesje et al., 2001; Seierstad et al., 2001; Nesje et al., 2005). This leads to increased glaciofluvial sediments (Hallet et al., 1995)

Process: snow avalanche

Event interval 3: 250 yrs. BP

Facies: B (top) and E (bottom)

The high grain count, the prevailing LIA combined with an documented increased avalanche activity by Nesje et al. (2007) and Vasskog et al. (2011).

Process: snow avalanche

Event interval 4: 360, 350 and 330 cal. yrs. BP

Facies: B

This event layers got deposited during a period of increased glacier activity and snow avalanche activity, the LIA, as documented by Nesje et al. (2007) and Vasskog et al. (2011).

Process: snow avalanche

Event interval 6: 550 to 470 cal. yrs. BP

Facies B.

This event interval is right at the beginning of the LIA. Nesje et al. (2007) and Vasskog et al. (2011) document increased snow avalanche activity.

Process: snow avalanche

Event interval 6: 700 yrs. BP

Facies: B

Based on the presented criteria, it can be concluded that this event interval probably presents only a single snow avalanche event.

Event interval 7: 850 cal. yrs. BP

Facies: B (top) and E (bottom)

Based on the presented criteria, the core image, and facies analysis, it can be concluded that this event was a snow avalanche, of which dropstones are deposited in the clay as well, which explains the spike in the 0,5 mm grain count plot.

Process: snow avalanche

Event interval 8: 1000 to 920 cal yrs. BP

Facies: B (bottom) and C (top)

This fining upwards sequence with a strong minerogenic part, showing a spike in the grain count plot (see figure 30). Although neither Nesje et al. (2007), nor Vasskog et al. (2011) document increased snow avalanche activity during this period, based on the sediment signature and the already mentioned criteria we conclude that this sediment package is deposited by snow avalanche. The reason for that can be a higher local snowfall and stronger winds which triggered the snow avalanche.

Event interval 9: 1550 to 1450 cal. yrs. BP

Facies: B

Nesje et al. (2007) and Vasskog et al. (2011) document increased snow avalanche activity during that time period. What is interesting about this event interval is that the 1 mm grain count is higher than other event intervals. The reason can be an event with a higher magnitude, can transport more larger grains.

We conclude that the process leading to the deposition of these sediments was a snow avalanche.

#### 5.2.4. Summary and answer to research question:

A total of 9 event assemblages have been identified through the interpretation of the results and comparison with previous work and climate shifts in the Holocene.

The identified processes for events which exceed a certain magnitude and are easily distinguishable have been snow avalanches. This concurs with the regional record from Nesje et al. (2007) and Vasskog et al. (2011).

Fluvial and glaciofluvial, in addition to organic and minerogenic background sedimentation, are the other identified processes, which deposit lake sediments in Kjøsnesfjorden.

### 5.3. Core 603-21-08 PC

#### 5.3.1. Age-Depth model

Seven radiocarbon samples were taken from the core (see chapter 4.3.2). One was taken before (174 cm) and after (170 cm) the light-grey layer in core 603-21-08 PC. Apparently, an error with the labelling during sampling or at the Poznan Radiocarbon Laboratory occurred and the results of the samples (Poz-148787 and Poz-148727) are exchanged. One sample was picked in the brown gyttja at 143 cm, one after the transition to the laminated silt at 122 cm and three in the laminated silt (85 cm, 50 cm and 25 cm).

#### 5.3.2. The use of lake sediments to analyse glacial activity.

This study uses lake sediments to define the glacial activity through various approaches: MS, LOI and geochemical variations (XRF). Both surrounding glaciers, Grovabreen and Jostedalsbreen, contribute glacier-derived sediments via meltwater channels and streams flowing into Kjøsnesfjorden (see maps of the area). Those meltwater streams transport large amounts of suspended clay and silt, produced by the glaciers through abrasion and transported by meltwater underneath. The amount of silt being deposited can be used as a



proxy for glacial activity. This assumption is based on Karlén & Denton (1976)'s approach, already discussed in the introduction (see chapter 1.1). Through the analysis of different geochemical elements through XRF analysis, a high-resolution record of the status of the glacier and its interaction with the climate was obtained. The redox-insensitive Ti (Croudace et al., 2006) has been proven to be a good proxy for glacial erosion, and therefore Bakke et al. (2009) and Wittmeier et al. (2015) link the semi-quantitatively measured titanium (Ti) concentration to glacial activity. This proxy and the other measurements will be discussed in the following chapters, and their uncertainties will be examined.

A certain number of climate anomalies occurred during the Holocene: HTM, "Finse-event", Neoglaciation, MCA and LIA. Kjøsnestjønnen is one of many lakes surrounding the Jostedalsglacier plateau and therefore its history and sediments are closely connected to the glacier's activity and the climate in the Holocene.

For this project, the normalised Ti, LOI and MS is used as a proxy for glacier activity. The performed PCA analysis (see chapter 4) Figure 31 shows other records about proxies used to analyse the glacier activity.

### 5.3.3. Interpretation of the sediment record

#### Unit A: 0 to 5300 yrs. BP

The Ti curve shows a steady glacier retreat until 75 yrs. BP, when the glacier advances again. It can therefore be concluded that either the results are wrong, which is quite unlikely since the rest of the record is well-usable, or the top of the sediment record are not available in this core. The results from the MS curve shows an increase in glacier activity from 3650 yrs. BP suggesting increased glacier activity (see result chapter 4.2.2). The LOI suggest the lowest amount of organic matter during the little Ice Age, a period of glacier advances on the Northern hemisphere that lasted from the late 15<sup>th</sup> to the late 19<sup>th</sup> century.

The medieval climate anomaly (MCA), in which glaciers were retreating can be documented in unit A.

The overall glacier activity decreases from 1000 to 4750 yrs. BP.

There are spikes representing glacier advance at 1300, 1900, 2200, 2400, 2600, 2700, 3000, 3400, 3600, 3900, 4100. The negative spikes representing a glacier retreat are at: 1600, 1750, 2100, 2300, 2500, 2800, 3200, 3750, 4200, 4300 yrs. BP.

There is a huge negative spike at 4550, which is a single piece of organic matter, which has probably been transported by a snow avalanche.

There are spikes representing glacier advance at 4100, 3900, 3600, 3400, 3000, 2700, 2600, 2400, 2200, 1900 and 1300 yrs. BP. The negative spikes representing glacier retreat at 4300, 4200, 3750, 3200, 2800, 2500, 2300, 2100, 1750 and 1600 yrs. BP.

The start of the neoglaciation period, in which the glacier is advancing, has a duration from 4750 yrs. BP until 5300 yrs. BP, when the LOI curve starts to decrease towards the present.

#### Uni B: 5300 to 7800 yrs. BP

The image of core 603-21-08 PC shows laminated layers of silt and gyttja from about 5200 to 7800 yrs. BP. When looking at the Ti curve and the core image, there are two sedimentation intervals visible. The first lasts from 5300 to 6500 yrs. BP. That interval has three positive spikes at 5500, 5700 and 6050 yrs. BP as well as two negative ones at 5600 and 5900 yrs. BP.

The second one starts at 6500 and lasts until 7500. The Ti curve shows two negative spikes at 6600 and 6800 yrs. BP.

The deglaciation continues and has its lowest point at 7300 yrs. BP, right after another much shorter cold period, shown by a spike and a slim light-grey layer with silt.

#### Uni C: 7700 to 7800 yrs. BP

A spike at 7800 cal. yrs. BP represents the “8,2 ka” or “Finse-Event”, a cold period caused by the collapse of the Laurentide ice sheet (Barber et. al, 1998) is interpreted as glacier activity.

Unit D: 7800 to 8300 yrs. BP

This unit shows layers of laminated silt and gyttja.

The lowest gyttja layer is at 8300 yrs. BP. The glacier has its lowest pre-Finse position at 7800 yrs. BP.

Unit E: 8300 to 9000 yrs. BP

This unit consists of laminated clay and shows three peaks of glacier advance at 8700, 8800 and 9000 yrs. BP.

### 5.3.4. Comparison of interpretation with previous glacier activity record

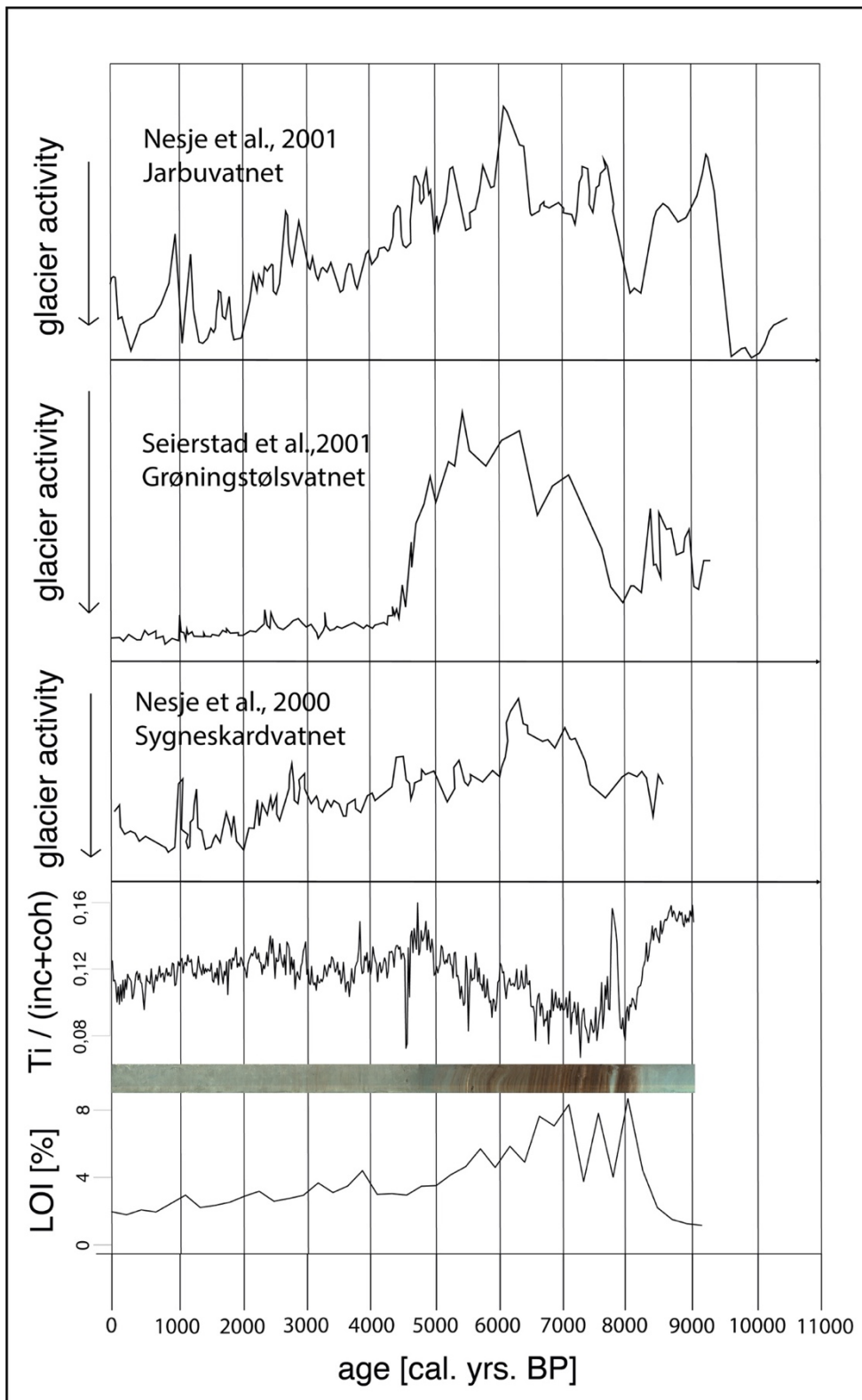


Figure 33 Comparison of previous records with core 603-21-08 PC's normalized Ti and LOI curve with the glacier activity plots of Nesje et al. (2000), Seierstad et al., (2001) and Nesje et al., (2001).

Figure 33 compares previous records with this project's normalised Ti and LOI curve. Their records and interpretations show a similar pattern in glacier activity in the timespan prior to the "Finse"-event, which is evident in each of those records. The radiocarbon ages for the "Finse"-event range from 8400 yrs. BP (Nesje et al., 2000), 8420 to 7800 cal. yrs. BP (Seierstad et al., 2001), 8400 to 8100 cal. yrs. BP (Nesje et al., 2001), 8200 to 7900 cal. yrs. BP (Nesje et al., 2005) and this project's range is 7700 to 7800 cal. yrs. BP.

The previous studies (Nesje et al. (2000), Seierstad et al. (2001) and Nesje et al. (2001)) document a temperature rise, followed by a steady increase in glacier activity.

In the sediment record of Nesje et al. (2000), Seierstad et al. (2001) and Nesje et al. (2001) a similar pattern of interlaying silt and gyttja like that in core 603-21-08 PC during the HTM is documented. Different ages for the lowest glacier activity are given by Nesje et al. (2000), Seierstad et al. (2001) and Nesje et al. (2001): 6300 yrs. BP, 5400 yrs. BP and 5200 yrs. BP. Results from this master project give the lowest glacier activity much earlier at 7000 yrs. BP.

Nesje et al. (2005) state that Jostedalbreen was melted from 8900 to 2000 cal. yr. BP.

After the HTM, Grovabreen's activity (Seierstad et al., 2001) is consistent, while Jostedalsbreen (Nesje et al., 2000; Nesje et al., 2001 and Nesje et al., 2005) has periods of high and low activity which is also documented in core 603-21-08 PC, but is continuously advancing since 7000 yrs. BP.

During the LIA, the glacier activity increased, and Nesje et al. (2001)'s record shows a spike in the presented composite (from Nesje et al., 1991; Nesje et al., 2000 and Nesje et al., 2001) Holocene glaciation curve.

Interestingly, the other previously mentioned records and this project's record don't show a significantly increased glacier activity and this might be because part of the sediment record is not present in this core.

### 5.3.5. Summary and answer to research question

All records show a decreasing glacier activity after 9000 yrs. BP, followed by a short period of glacier activity (Finse-event). Afterwards, the glacier activity decreases further until the point of lowest activity at 7300 yrs. BP. In sediment cores from lake Kjøsnesfjorden, gyttja and silt could still be found at that time.

After 7000 yrs. BP the glacier activity increased and the glacier advanced, evident in overall decreasing LOI weights and an increasing Ti-value.

Nesje et al. (2000), Seierstad et al. (2001), Nesje et al. (2001) and Nesje et al. (2005) and this project as well state that the whole period was characterized by cold as well as milder periods, each ranging 100 to 200 years.

Even though there are no definite radiocarbon dating results, it can be concluded that unit E (laminated silt) was deposited after Kjøsnesfjorden was deglaciated from the Scandinavian ice sheet at 10 365 cal. yrs. BP.

The depositional environment, which led to the deposition of unit B showing the laminated silt and gyttja gives room for speculation. While Nesje et al. (2005) proposes that, according to ELA calculations, Jostedalsbreen was melted away, we propose that the glacier was still present and it was probably a lot smaller than today. One reason, the laminations containing glacial sediments is that sedimentation regime on the Jostedalsbreen plateau has shifted depending on the actual size of the glacier and climatic factors, such as precipitation, wind direction and intensity.

## 6. Conclusion

The presented analysis of lake sediments from Kjøsnestjorden in Western Norway investigated avalanche and glacier deposits, and the impact of climate during the Holocene.

Kjøsnestjorden is a great research ground for paleoclimatic change due to its steep slopes, which leads to records of mass wasting events. The surrounding glaciers, Grovabreen and Jostedalbreen provide a sediments deposited in Kjøsnestjorden.

Several scientific methods have been used to collect data during the field survey: bathymetric mapping, CHIRP mapping and coring. Two sediment cores have been further analysed using laboratory methods, including logging, XRF- scanning, MS,  $^{14}\text{C}$ -dating, LOI and CT- scanning.

The achieved data was further processed using PCA to distinguish between minerogenic and non-minerogenic units in core 603-21-08 PC.

It is evident from the performed PCA that the elements Ca, Fe, Si and Ti reflect minerogenic sedimentary input. It is concluded that input of minerogenic sediment during the Neoglacial period has been mainly driven by glacier activity.

After the deglaciation of Kjøsnestjorden, the "Finse-event" led to a sudden increase in glacier activity, followed by the HTM, a mild period with less glacier activity at the beginning. At 7000 yrs. BP, the glaciers steadily advance, at 5300 yrs. BP, the end of the HTM, the sedimental record of core 603-21-08 PC is only minerogenic and therefor glacial origin.

The impact of the surrounding glaciers on the landslide activity around Kjøsnestjorden is evident in 7 of 9 snow avalanche event intervals, recorded in core 603-21-01 PC and occurred during the LIA and the 20<sup>th</sup> century. The other two snow avalanches are recorded at 1000 and 1550 yrs. BP. In addition, fluvial and glacially driven sedimentary processes have been identified.

This project adds to a fuller understanding of the glacier history of Jostedalsbreen and Grovabreen by providing a detailed sediment analysis including XRF-analysis, MS measurements and LOI-measurements in addition to an established age-depth model.

The newly created bathymetric map (with recent CHIRP profiles) of Kjøsnestjorden, the identified slope and sedimentary processes, combined with the sedimentary record of climate changes during the Holocene, increase awareness of the effects of climate change on our environment.



## 7. Future

Kjøsnestfjorden and the Jostedalbreen plateau provide an exciting research field for climate change studies, slope processes and lake sediments, of which this project has highlighted certain aspects and approaches.

Future research areas can include:

- 1.) An in-depth grain-size analysis of the laminations, in combination with surface-exposure dating in core 603-21-08 PC to get a better understanding of Jostedalbreen's glacier history during the HTM. This can be combined with ground penetrating radar measurements of the surrounding plateau, including the glacier Jostedalbreen to link the glacial sediments to the geomorphology.
  
- 2.) Additional dating and grain-size measurements on the event layers of the presented core 603-21-01 PC and the other cores were taken during the field survey.
  
- 3.) Being deglaciated since 9500 yrs. BP, Kjøsnestfjorden can provide a slope process record displaying almost the entire Holocene, which can then be linked to climatic changes in the Holocene and therefore future climate studies can be done, when the Earth's average temperature rises a few degrees, and the glaciers retreat further.

## 8. References:

- Aa, A. R. (1995). "Topographic control of equilibrium-line altitude depression on reconstructed 'Little Ice Age' glaciers, Grovabreen, western Norway." The Holocene **6**(1): 82-89.
- Aa, A. R., et al. (2022). "Holocene debris flows and snow avalanches in Anest? Isdalen, western Norway-recorded from lake deposits and colluvial fans." Norwegian Journal of Geology.
- Andreassen, L. M., et al. (2020). "Glacier change in Norway since the 1960s—an overview of mass balance, area, length and surface elevation changes." Journal of glaciology **66**(256): 313-328.
- Bakke, J., et al. (2005). "Glacier fluctuations, equilibrium-line altitudes and palaeoclimate in Lyngen, northern Norway, during the Lateglacial and Holocene." The Holocene **15**(4): 518-540.
- Bakke, J., et al. (2010). "A complete record of Holocene glacier variability at Austre Okstindbreen, northern Norway: an integrated approach." Quaternary Science Reviews **29**(9-10): 1246-1262.
- Bakke, J., et al. (2009). "Rapid oceanic and atmospheric changes during the Younger Dryas cold period." Nature Geoscience **2**(3): 202-205.
- Bakke, J., et al. (2005). "Utilizing physical sediment variability in glacier-fed lakes for continuous glacier reconstructions during the Holocene, northern Folgefonna, western Norway." The Holocene **15**(2): 161-176.
- Bakke, J., et al. (2013). "Numerical analyses of a multi-proxy data set from a distal glacier-fed lake, Sørsendalsvatn, western Norway." Quaternary Science Reviews **73**: 182-195.
- Barber, D., et al. (1999). "Forcing of the cold event of 8,200 years ago by catastrophic drainage of Laurentide lakes." Nature **400**: 344-348.
- Berger, A. (1978). "Long-term variations of caloric insolation resulting from the Earth's orbital elements." Quaternary research **9**(2): 139-167.
- Birks, H. (2007). PLANT MACROFOSSIL INTRODUCTION. Encyclopedia of Quaternary Science. **3**: 2266-2288.
- Bjune, A. E., et al. (2005). "Holocene mean July temperature and winter precipitation in western Norway inferred from palynological and glaciological lake-sediment proxies." The Holocene **15**(2): 177-189.

- Blaauw, M. (2010). "Methods and code for 'classical' age-modelling of radiocarbon sequences." Quaternary Geochronology **5**(5): 512-518.
- Blaauw, M. and J. Christen (2011). "Flexible Paleoclimate Age-Depth Models Using an Autoregressive Gamma Process." Bayesian Analysis **6**: 457-474.
- Bradley, R. S. (1999). Paleoclimatology: Reconstructing Climates of the Quaternary: Third Edition.
- Briffa, K. R., et al. (1998). "Trees tell of past climates: But are they speaking less clearly today?" Philosophical Transactions of the Royal Society of London Series B Containing Papers of a Biological Character (1896-1934) **353**: 65-73.
- CASELDINE, C. J. and J. A. MATTHEWS (1987). "Podzol development, vegetation change and glacier variations at Haugabreen, southern Norway." Boreas **16**(3): 215-230.
- Color, M. (1994). Munsell Soil Color Charts. 1994.
- Cronin, T. M. (2010). Paleoclimates: Understanding Climate Change Past and Present, Columbia University Press, New York.
- Croudace, I., et al. (2006). "ITRAX: Description and Evaluation of a New Multi-Function X-ray Core Scanner." Geological Society, London, Special Publications **267**: 51-63.
- Cuffey, K. M. and W. S. B. Paterson (2010). The physics of glaciers, Academic Press.
- Dahl, S. O., et al. (2002). "Timing, equilibrium-line altitudes and climatic implications of two early-Holocene glacier readvances during the Erdalen Event at Jostedalbreen, western Norway." The Holocene **12**(1): 17-25.
- Dean, W. E. (1974). "Determination of carbonate and organic matter in calcareous sediments and sedimentary rocks by loss on ignition; comparison with other methods." Journal of Sedimentary Research **44**(1): 242-248.
- Gaillard, M.-J. and H. Birks (2007). PLANT MACROFOSSIL METHODS AND STUDIES | Paleolimnological Applications: 2337-2356.
- Gilli, A., et al. (2013). "Lake Sediments as Archives of Recurrence Rates and Intensities of Past Flood Events." Adv. Glob. Change Res. **47**.
- Gjerde, M., et al. (2018). "Holocene multi-proxy environmental reconstruction from lake Hakluytvatnet, Amsterdamøya Island, Svalbard (79.5 N)." Quaternary Science Reviews **183**: 164-176.
- Hallet, B., et al. (1996). "Rates of erosion and sediment evacuation by glaciers: A review of field data and their implications." Global and Planetary Change **12**(1-4): 213-235.

Hanssen-Bauer, I., et al. (2009). "Klima i Norge 2100." Bakgrunnsmateriale til NOU Klimatilpassing., Norsk klimasenter, Oslo, Norway.

Hardeng, J., et al. (2022). "Lake sediments from southern Norway capture Holocene variations in flood seasonality." Quaternary Science Reviews **290**: 107643.

Hardeng, J., et al. (2022). "Lake sediments from southern Norway capture Holocene variations in flood seasonality." Quaternary Science Reviews **290**: 107643.

Hesjedal, M. (2022). Kartlegging av skredavsetninger langs Kjørnesfjorden i et klimaperspektiv. Mapping of avalanche deposits along the Kjørnesfjord in a climate perspective, The University of Bergen.

Hurrell, J. W. (1995). "Decadal trends in the North Atlantic Oscillation: Regional temperatures and precipitation." Science **269**(5224): 676-679.

Hurrell, J. W., et al. (2003). "An overview of the North Atlantic oscillation." Geophysical Monograph-American Geophysical Union **134**: 1-36.

Karlen, D., et al. (1988). "Aerial accumulation and partitioning of nutrients by corn." Agronomy Journal **80**(2): 232-242.

Karlén, W. and G. H. DENTON (1976). "Holocene glacial variations in Sarek National Park, northern Sweden." Boreas **5**(1): 25-56.

Klakegg, O. (1981). Kvartærgeologiske studier i Jølster, Sogn og Fjordane : 1 : Tekst og tabellar. Bergen.

Klakegg, O. and N. Rye (1990). "Tilting of lake shorelines in Jølstravatnet, western Norway, caused by glacioisostatic rebound." Norsk geologisk tidsskrift **70**: 47-59.

Kylander, M. E., et al. (2011). "High-resolution X-ray fluorescence core scanning analysis of Les Echets (France) sedimentary sequence: new insights from chemical proxies." Journal of Quaternary Science **26**(1): 109-117.

Matero, I. S. O., et al. (2017). "The 8.2 ka cooling event caused by Laurentide ice saddle collapse." Earth and Planetary Science Letters **473**: 205-214.

Mons Kvamme, A. O., PA Aarestad (1989). Botanical investigations in Jostedal. Report 47. M. Kvamme. Bergen, Botanical Institute, University of Bergen: 166 - 202.

Nesje, A. (1992). "A Piston Corer for Lacustrine and Marine Sediments." Arctic and Alpine Research **24**(3): 257-259.

Nesje, A. (1992). "Younger dryas and holocene glacier fluctuations and equilibrium-line altitude variations in the Jostedalsbre region, western Norway." Climate Dynamics **6**(3): 221-227.

- Nesje, A. (2009). "Latest Pleistocene and Holocene alpine glacier fluctuations in Scandinavia." Quaternary Science Reviews **28**(21-22): 2119-2136.
- Nesje, A., et al. (2007). "A continuous, high-resolution 8500-yr snow-avalanche record from western Norway." The Holocene **17**(2): 269-277.
- Nesje, A. and S. O. Dahl (1991). "Late Holocene glacier fluctuations in Bevringsdalen, Jostedalbreen region, western Norway (ca 3200-1400 BP)." The Holocene **1**(1): 1-7.
- Nesje, A. and S. O. Dahl (2001). "The Greenland 8200 cal. yr BP event detected in loss-on-ignition profiles in Norwegian lacustrine sediment sequences." Journal of Quaternary Science: Published for the Quaternary Research Association **16**(2): 155-166.
- Nesje, A. and S. O. Dahl (2003). "The 'little ice age'—only temperature?" The Holocene **13**(1): 139-145.
- Nesje, A., et al. (2000). "The lacustrine sedimentary sequence in Syngneskardvatnet, western Norway: a continuous, high-resolution record of the Jostedalbreen ice cap during the Holocene." Quaternary Science Reviews **19**(11): 1047-1065.
- Nesje, A., et al. (2008). "The 'Little Ice Age' glacial expansion in western Scandinavia: summer temperature or winter precipitation?" Climate Dynamics **30**: 789-801.
- Nesje, A. and M. Kvamme (1991). "Holocene glacier and climate variations in western Norway: evidence for early Holocene glacier demise and multiple Neoglacial events." Geology **19**(6): 610-612.
- Nesje, A., et al. (1991). "Holocene glacial and climate history of the Jostedalbreen region, Western Norway; evidence from lake sediments and terrestrial deposits." Quaternary Science Reviews **10**(1): 87-114.  
100–150 m indicates a mean temperature decline from the present of ca. 0.5–1°C.
- Nesje, A., et al. (2001). "Holocene glacier fluctuations of Flatebreen and winter-precipitation changes in the Jostedalbreen region, western Norway, based on glaciolacustrine sediment records." The Holocene **11**(3): 267-280.
- Nielsen, P. R., et al. (2016). "Holocene aeolian sedimentation and episodic mass-wasting events recorded in lacustrine sediments on Langøya in Vesterålen, northern Norway." Quaternary Science Reviews **148**: 146-162.
- Olsson, I. U. (1968). "Modern aspects of radiocarbon datings." Earth-Science Reviews **4**: 203-218.
- Orsi, T. H. (1995). "Computed Tomography of Macrostructure and Physical Property Variability of Seafloor Sediments." Oceanography **8**(2): 61-64.

- Orsi, T. H., et al. (1994). "X-ray computed tomography; a nondestructive method for quantitative analysis of sediment cores." Journal of Sedimentary Research **64**(3a): 690-693.
- Pendleton, R. L. and D. Nickerson (1951). "Soil colors and special Munsell soil color charts." Soil Science **71**(1): 35-44.
- R. Thompson, R. W. B., P.E. O'Sullivan, F. Oldfield (1975). "Magnetic susceptibility of lake sediments." Limnology and Oceanography **20**(5).
- Reimer, P. J., et al. (2016). "IntCal13 and Marine13 Radiocarbon Age Calibration Curves 0–50,000 Years cal BP." Radiocarbon **55**(4): 1869-1887.
- Renssen, H., et al. (2012). "Global characterization of the Holocene Thermal Maximum." Quaternary Science Reviews **48**: 7-19.
- Røthe, T. O., et al. (2019). "Wintertime extreme events recorded by lake sediments in Arctic Norway." The Holocene **29**(8): 1305-1321.
- Rye, N., et al. (1987). "The Late Weichselian ice sheet in the Nordfjord – Sunnmøre area and deglaciation chronology for Nordfjord, western Norway." Norsk Geografisk Tidsskrift - Norwegian Journal of Geography **41**(1): 23-43.
- Sabatier, P., et al. (2022). "A review of event deposits in lake sediments." Quaternary **5**(3): 34.
- Seierstad, J., et al. (2001). "Holocene glacier fluctuations of Grovabreen and Holocene snow-avalanche activity reconstructed from lake sediments in Grningstlsvatnet, western Norway." The Holocene **12**(2): 211-222.
- Sletten, K., et al. (2003). "Holocene debris flows recognized in a lacustrine sedimentary succession: sedimentology, chronostratigraphy and cause of triggering." The Holocene **13**(6): 907-920.
- Støren, E., et al. (2010). "Identifying the sedimentary imprint of high-frequency Holocene river floods in lake sediments: Development and application of a new method." Quaternary Science Reviews **29**: 3021-3033.
- Støren, E., et al. (2016). "Magnetic and geochemical signatures of flood layers in a lake system." Geochemistry Geophysics Geosystems **17**.
- Sturm, M. and A. Matter (1978). "Turbidites and varves in Lake Brienz (Switzerland): deposition of clastic detritus by density currents." Modern and ancient lake sediments: 147-168.
- Thompson, R., et al. (1975). "Magnetic susceptibility of lake sediments." Limnology and Oceanography **20**(5): 687-698.

UWITEC Uwitec USC 09000, UWITEC GmbH Weißensteinstraße 30, 5310 Mondsee, Austria: 2.

van der Bilt, W., et al. (2016). "Glacier-fed lakes as palaeoenvironmental archives." Geology Today **32**: 213-218.

van der Bilt, W., et al. (2018). "Novel sedimentological fingerprints link shifting depositional processes to Holocene climate transitions in East Greenland." Global and Planetary Change **164**.

van der Bilt, W. G. M., et al. (2015). "Reconstruction of glacier variability from lake sediments reveals dynamic Holocene climate in Svalbard." Quaternary Science Reviews **126**: 201-218.

Vasskog, K., et al. (2011). "A Holocene record of snow-avalanche and flood activity reconstructed from a lacustrine sedimentary sequence in Oldevatnet, western Norway." The Holocene **21**(4): 597-614.

Wittmeier, H., et al. (2015). "Reconstructing Holocene glacier activity at Langfjordjøkelen, Arctic Norway, using multi-proxy fingerprinting of distal glacier-fed lake sediments." Quaternary Science Reviews **114**: 78-99.

Xu, M., et al. (2015). "Early and late Holocene sediment yield of Austdalsbreen glacier, southwest Norway." Geomorphology **246**: 277-289.

Zemp, M., et al. (2015). "Historically unprecedented global glacier decline in the early 21st century." Journal of glaciology **61**(228): 745-762.

NVE glacier report, 2022

Mastersizer 3000 Brochure. (2013). Malvern Panalytical.

<https://physicsopenlab.org/2016/02/24/diy-xrf-spectrometry/>